Physical and Biogeochemical Responses to Freshwater-Induced Thermohaline Variability in a Zonally Averaged Ocean Model

Olivier Marchal, Thomas F. Stocker, and Fortunat Joos

Climate and Environmental Physics, Physics Institute, University of Bern

Freshwater perturbation experiments are conducted with a latitude-depth, circulation-biogeochemistry ocean model coupled to an energy balance model of the atmosphere. The aim is to identify potential effects of different changes of the Atlantic thermohaline circulation (THC). Strong THC reductions (> 50%) lead to cooling at high northern latitudes and warming in the southern hemisphere. For moderate reductions, however, cooling in the north is not accompanied by temperature changes in the south. These results are discussed in relation with a recent synchronization of isotopic records from Greenland and Antarctic ice cores based on methane, which documents north-south thermal antiphasing during the largest Greenland $\delta^{18}O$ oscillations and no clear Antarctic counterparts during the other, shorter oscillations of the last glacial period. Simulations show that strong THC reductions result in PO_4 enrichment and $\delta^{13}C$ depletion below 1 km in the North Atlantic reaching, on average, about 0.5 mmol m^{-3} and -0.3‰ for a complete THC collapse. These chemical and isotopic changes are due to an imbalance between organic matter oxidation and import of nutrient-poor waters from the northern North Atlantic. The THC reductions also lead to a drop in $\delta^{13}C$ air-sea disequilibrium in the Atlantic where the surface waters stay longer in contact with the atmosphere. Thus, in the upper kilometer, cold waters in the northern North Atlantic become isotopically heavier (by more than 1‰), whereas warm waters further south become slightly lighter (~ -0.2‰). The simulated chemical and isotopic shifts are much smaller below 1 km in the South Atlantic and Southern Ocean. These results indicate that the same circulation change could produce completely different PO_4 and $\delta^{13}C$ anomalies at different locations and depths in the Atlantic and Southern Ocean. This might have strong implications for the interpretation of marine Cd/Ca and $\delta^{13}C$ sediment records obtained from different oceanic regions.

1. INTRODUCTION

A major area of current climate research is the study of the large, millennial-scale variability observed in many paleoclimate records. The prominent and abrupt $\delta^{18}O$ oscillations observed in Greenland ice cores during the

Mechanisms of Global Climate Change at Millennial Time Scales
Geophysical Monograph 112

last glacial period [*Dansgaard et al.*, 1982; *Oeschger et al.*, 1984; *Johnsen et al.*, 1992] prompted a search for such variability in records from various parts of the climate system. When translated into temperature (T) changes from the modern spatial relationship between the annual mean snow $\delta^{18}O$ and T in polar regions, these "Dansgaard-Oeschger" (D-O) events correspond to warming-cooling cycles with an amplitude of $\sim$ 7°C [*Johnsen et al.*, 1992]. The estimated temperature changes are even larger if the relationship is calibrated by borehole temperature measurements [*Johnsen et al.*, 1995; *Cuffey and Clow*, 1997]. The best investigated abrupt oscillation in Greenland $\delta^{18}O$ records is the Younger Dryas cold event (YD), dated by annual layer counting to between 12,700±100 yr BP–11,550±70 yr BP in the GRIP ice core [*Johnsen et al.*, 1992] and 12,940±260 yr BP–11,640±250 yr BP in the GISP2 ice core [*Alley et al.*, 1993]. The fractionation of nitrogen and argon isotopes at the transition from the YD to the Preboreal in the GISP2 core indicates that Central Greenland was 15±3°C colder during the Younger Dryas than today [*Severinghaus et al.*, 1998].

There has been a long controversy about whether the Younger Dryas has been a global event or not. Continental pollen sequences reveal that the YD affected western Europe and eastern North America, but do not provide definitive evidence of the event in other regions [*Peteet*, 1995]. Gas measurements on polar ice cores, on the other hand, document that the atmospheric CH_4 concentration followed Greenland $\delta^{18}O$ shifts of the last glaciation, including the YD [*Chappellaz et al.*, 1993; *Brook et al.*, 1996]. These measurements suggest that the D-O events were at least hemispheric in extent, as a main source of atmospheric CH_4 during the last glacial period was tropical wetlands [*Chappellaz et al.*, 1993]. Climatic records from glacier stands in New Zealand [*Denton and Hendy*, 1994] and Southern Chile [*Lowell et al.*, 1995] document notable glacier advances during the last deglaciation. If glacier stands are faithful recorders of temperature only, then the advances come close in time to the Younger Dryas. *Denton and Hendy* [1994] concluded thus, that Younger Dryas must be a cold event of global extent, possibly with an enhanced signal in the north. However, uncertainties in the time scale and interpretation of wood remains in moraines [*Mabin*, 1996] as well as recent analyses of pollen assemblages [*Singer et al.*, 1998] do not support this conclusion.

Measurements of the $^{18}O/^{16}O$ ratio of O_2 and of the CH_4 content in air trapped in ice permits the synchronization of climate records from both polar regions. *Bender et al.* [1994a] placed the δD record from Vostok (East Antarctica) and the GISP2 $\delta^{18}O$ record on a common chronology based on $^{18}O/^{16}O$ measurements on O_2. They showed that the last glacial Greenland interstadials longer than $\sim$ 2,000 yr have counterparts in Antarctica. The same approach was adopted by *Sowers and Bender* [1995] who demonstrated that warming in the Byrd $\delta^{18}O$ record (West Antarctica) began approximately 3,000 yr before the onset of the warm Bølling epoch in the GISP2 $\delta^{18}O$ record. Past changes in the $^{18}O/^{16}O$ ratio of atmospheric oxygen, however, were relatively small, which prevents the determination of the phase relationships between Greenland and Antarctica during the abrupt climate changes of the last glacial period [*Bender et al.*, 1994b]. By contrast, fast CH_4 variations during this period permits a fit of ice core CH_4 records from both polar regions to ± 200 yr [*Blunier et al.*, 1998]. *Blunier et al.* [1997] and *Blunier et al.* [1998] used CH_4 measured in GRIP, Byrd, and Vostok ice cores to put the isotopic records from these different sites on the same timescale. They found a conspicuous antiphase relationship between the high northern and southern latitudes during the prominent Greenland $\delta^{18}O$ events 8 and 12 [*Dansgaard et al.*, 1993] and the Bølling/Allerød/YD sequence. However, this relationship does not hold for all of the 14 D-O cycles of the last 50,000 years, as the other, shorter Greenland $\delta^{18}O$ events do not have clear counterparts in Antarctica. The possible wide geographic expression of the YD and other D-O events has profound implications for our understanding of climate dynamics, as it provides insight into the propagation of anomalies caused by abrupt changes in the atmosphere-ocean-ice system.

A possible cause of the millennial-scale, warming-cooling cycles of the last glacial period is changes in the Atlantic thermohaline circulation (THC) [*Broecker et al.*, 1985]. These changes may have been triggered, in turn, by the discharge of low-density meltwater from the big ice sheets which covered the northern hemisphere during this period. A major support to the THC hypothesis comes from various model simulations showing that a reduction of the THC causes a cooling in the North Atlantic region [*Wright and Stocker*, 1993; *Manabe and Stouffer*, 1995; *Manabe and Stouffer*, 1997; *Fanning and Weaver*, 1997; *Mikolajewicz et al.*, 1997; *Schiller et al.*, 1997]. Furthermore, consistent with polar isotopic records, climate models point to an antiphase relationship, whereby the south exhibits a warming when the North cools abruptly and vice versa (for a review see *Stocker*, 1999). The mechanism is simple: an active THC in the Atlantic draws heat from the Southern Ocean into the Atlantic basin [*Crowley*, 1992; *Stocker et al.*, 1992a]. If it is switched off, the excess heat tends to warm subsurface and surface waters in the South Atlantic and Southern Ocean. A sudden initiation of the THC, on the other hand, should lead to a cooling in the south. If the mechanism is indeed operating, this behaviour should be particularly present during the transitions into and out of the YD and other, similarly strong events.

Deep sea records of fossil benthic foraminiferal Cd/Ca and $\delta^{13}C$, however, have led to contradictory conclusions regarding the state of the THC during the Younger Dryas event [*Boyle and Keigwin*, 1987; *Keigwin et al.*, 1991; *Keigwin and Lehman*, 1994; *Jansen and Veum*, 1990; *Veum et al.*, 1992; *Charles and Fairbanks*, 1992; *Bard et al.*, 1994]. Data of the difference between benthic and planktonic foraminifera ^{14}C ages are still too sparse to constrain ventilation changes during this event [*Adkins and Boyle*, 1997]. The apparent inconsistency between various sediment records could be due to the coarse temporal resolution and sampling frequency in some of the deep sea cores [*Boyle*, 1995]. Other possible causes for such inconsistencies are that these records come from different locations and depths and that different paleocirculation proxies, such as the foraminiferal Cd/Ca, $\delta^{13}C$, and $\Delta^{14}C$, are influenced by distinct oceanic processes [*Jansen and Veum*, 1990].

In this paper we examine the effect of large and small freshwater-induced changes in the Atlantic thermohaline circulation on the climatic coupling between the two hemispheres and on the distribution of $\Delta^{14}C$, PO_4, and $\delta^{13}C$ in the deep sea. We conduct various freshwater perturbation experiments with a latitude-depth, circulation-biogeochemistry ocean model [*Marchal et al.*, 1998a] coupled to an energy balance model of the atmosphere. The ocean model accounts for the main features of the thermohaline circulation and biological cycling which govern the large-scale distribution of major chemical and isotopic tracers. It allows us to perfom extensive and millennial-scale numerical integrations.

2. MODEL DESCRIPTION

The model includes physical and biogeochemical components. These components have been detailed in previous publications and we give only a brief description here. The ocean physical component is the zonally averaged circulation model of *Wright and Stocker* [1992] with the dynamical closure of *Wright et al.* [1998]. The Atlantic, Indian, and Pacific basins are represented individually and connected by a well-mixed Southern Ocean (for model grid see *Stocker and Wright*, 1996). The set of circulation parameters adopted here produces a reasonable agreement with the basin mean vertical profiles of temperature, salinity, and $\Delta^{14}C$ of dissolved inorganic carbon observed in the modern oceans [*Marchal et al.*, 1998a]. The ocean component is coupled to an energy balance model of the atmosphere [*Stocker et al.*, 1992a] and to a thermodynamic sea ice model (described in *Wright and Stocker*, 1993) in order to permit transitions between different climatic states (for parameters see *Wright and Stocker*, 1993).

The ocean biogeochemical component is a description of the cycles of organic carbon and $CaCO_3$ [*Marchal et al.*, 1998a]. Nine tracers are considered: phosphate (taken as the biolimiting nutrient), dissolved inorganic carbon (DIC), alkalinity (ALK), labile dissolved organic carbon (DOC_l), dissolved oxygen, and ^{13}C and ^{14}C in DIC and in DOC_l. River input and sediment burial are omitted, i.e. all the organic carbon and $CaCO_3$ produced in the euphotic zone (top 100 m) are entirely recycled in the water column below. The production of organic carbon exported from the euphotic zone (J_{org}) depends on the local PO_4 availability via Michaelis-Menten kinetics:

$$J_{org} = J_{pot} \cdot \frac{PO_4}{K_{PO_4} + PO_4}, \tag{1}$$

where J_{pot} is a potential export production diagnosed from the spin-up and K_{PO_4} is a half-saturation constant for PO_4 uptake [*Marchal et al.*, 1998b]. The export production is partitioned between fast sinking particulate organic carbon (POC) and DOC_l, both are recycled below the euphotic zone. POC is remineralized without delay according to a spatially uniform vertical profile consistent with sediment trap data [*Bishop*, 1989], whereas DOC_l is oxidized assuming first-order kinetics. The air-sea fluxes of the carbon isotopes are calculated with a constant CO_2 transfer coefficient (Appendix C). The biogeochemical parameters were constrained so as to produce a reasonable fit to the distributions of PO_4, apparent oxygen utilization, DIC, ALK, and $\delta^{13}C$ (of DIC) observed in the modern oceans [*Marchal et al.*, 1998a].

The land biogeochemical component is a 4-pool land biosphere model [*Siegenthaler and Oeschger*, 1987]. We use this model for ^{13}C and ^{14}C perturbations in order to account for the relatively large dilution effect caused by the land biosphere. The biospheric fluxes of organic carbon and the CO_2 fluxes between the land biosphere and the atmosphere are kept constant. Thus we assume no changes in carbon storage and productivity on land [*Marchal et al.*, 1998b]. The ocean and the land biosphere exchange $^{12}CO_2$, $^{13}CO_2$, and $^{14}CO_2$ via the atmosphere which is considered well mixed with respect to these isotopes. Throughout the paper the term anomaly is used for any variable to denote the difference compared to the initial model steady state.

3. RESULTS

3.1. Physical Changes during Abrupt Events

The initial model steady state is characterized by a maximum rate of thermohaline overturning in the Atlantic of about 24 Sv (1 Sv = 10^6 m^3 s^{-1}; left panel in Fig. 1a). We simulate water masses [*Stocker et al.*, 1992b], conservative "colors" with specified origin of formation, in order to help the interpretation of $\Delta^{14}C$, PO_4, and $\delta^{13}C$ in the transient experiments. These water masses are designated North Atlantic Deep Water (formed between 55°N–80°N), Central Water (47.5°S–32.5°N), and Southern Ocean Water (70°S–47.5°S). In the initial steady state NADW dominates the deep Atlantic (Fig. 1b). NADW is sandwiched between two components of SOW: bottom waters formed along the Antarctic perimeter (70°S–62.5°S) and intermediate waters formed between 62.5°S–47.5°S (Fig. 1c). Central Water is essentially confined between 50°S–40°N in the Atlantic, with the 80% contour located above 250 m (Fig. 1d).

Different strengths of the THC are obtained by applying a freshwater flux anomaly (FFA) at the surface between 32.5°N–45°N in the Atlantic. We assume that the FFA follows a linear increase and then a linear decrease at the same rate r (Sv kyr^{-1}). The total volume of freshwater released, $V = 6 \cdot 10^6$ km^3, is the same in all the experiments and corresponds to a sea level rise of $\sim$ 17 m. Thus, the experiments differ only by the duration D of the FFA, or equivalently, by the rate of the FFA $r = 4V/D^2$.

A series of experiments demonstrates the sensitivity of the THC and water mass distribution in the Atlantic to the rapidity of the freshwater perturbation. A slow FFA has a relatively minor impact on the THC as it does not permit the development of a low-density cap in the North Atlantic region (Fig. 2). However, a threshold exists (corresponding to $r \sim 0.4$ Sv kyr^{-1} in our model) beyond which the FFA is sufficiently rapid to reduce drastically deep water formation and the thermohaline overturning rate in this region. NADW retreats, whereas SOW becomes more abundant in the deep Atlantic for a greater reduction of the THC (Fig. 1b–c). The reduced influence of NADW and the advance of waters of southern origin are due to the altered buoyancy contrast between high latitude surface waters when a low-density cap develops in the North Atlantic [*Stocker et al.*, 1992b]. Similarly, the Central Water remains confined in the upper water column in the North Atlantic, but reaches deeper levels south of the equator (Fig. 1d).

A hypothesis to explain the variable climate coupling between the two hemispheres [*Blunier et al.*, 1998] is that strong reductions of the THC occurred during prominent D-O events and that only partial shutdowns of the THC occurred during shorter D-O events [*Stocker*, 1999]. A partial shut-down is either a reduction in thermohaline overturning strength or a more southward change in convection location, both with the net result of a decreased heat supply by the THC to the North Atlantic region.

We test this hypothesis using our simplified, coupled ocean-atmosphere model. For illustration, we consider two cases: a partial reduction of the THC (experiment E2 where the THC drops from 24 Sv to 12 Sv) and a complete shut-down (E4 with THC dropping to 3 Sv). In the two cases heat accumulates in the South Atlantic which leads to a subsurface warming (Fig. 3a–b), confirming the concept explained by *Crowley* [1992]. A warming also occurs in the Indian and Pacific as deep water formation in the North Atlantic is the main mechanism adding cold water to the interior to counter the effect of vertical mixing. The partial reduction of the THC has a maximum subsurface warming in the top kilometer at $\sim$ 10°N in the Atlantic (Fig. 3a) while for the complete shut-down, the maximum warming is located in the same depth interval, but around 40°S (Fig. 3b). The former is in remarkable agreement with the temperature anomalies in a freshwater experiment with a coupled atmosphere-ocean, three-dimensional circulation model showing a partial shutdown [*Manabe and Stouffer*, 1997]. We note that the distribution of temperature anomaly in experiments E1 and E4 is qualitatively similar to that in experiments E2 and E4, respectively (maximum subsurface warming in E1, however, is in the North Atlantic).

The present model also simulates the changes in the zonally averaged surface air temperature, T_{atm}. It is clear that temperature changes over the northern North Atlantic are locally underestimated, because the model is zonally averaged. The two experiments show that the qualitative response of T_{atm} is also strongly dependent on the intensity of the THC reduction. A partial reduction leads to a cooling in the northern hemisphere only

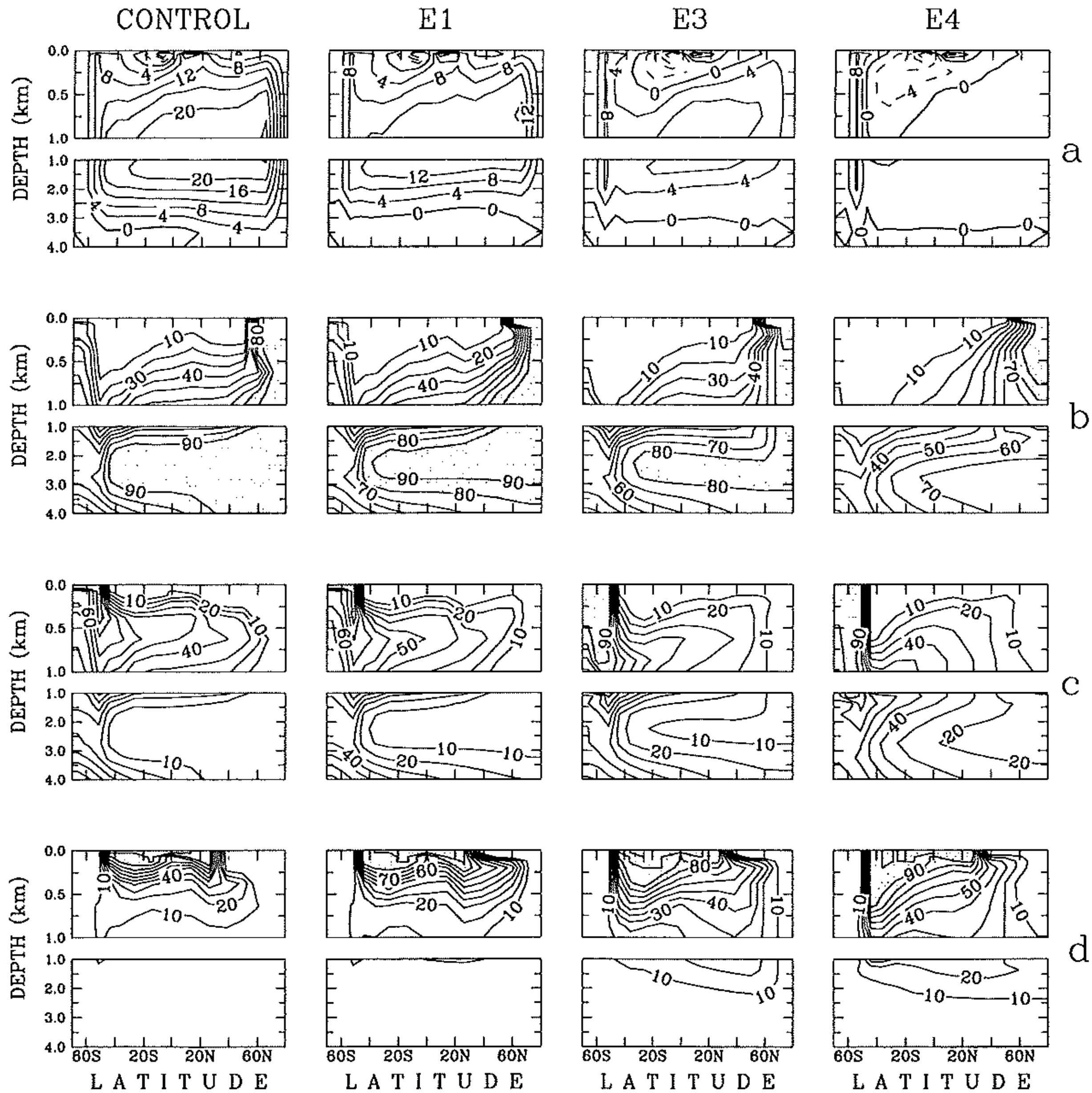

Figure 1. Latitude-depth distribution in the Atlantic of (a) the stream function (in Sv, 1 Sv = 10^6 m^3 s^{-1}) and (b–d) major water masses (%) at the initial model steady state (1st column) and in transient experiments E1 (2nd col.), E3 (3rd col.), and E4 (4th col.). The circulation response to freshwater flux anomaly (FFA) in E2 is similar to that in E3 (Fig. 2). The water masses are (b) North Atlantic Deep Water (formed between 55°N–80°N), (c) Southern Ocean Water (70°S–47.5°S), and (d) Central Water (47.5°S–32.5°N). The duration of the FFA is 2500 yr, 1350 yr, and 1000 yr in experiments E1, E3, and E4, respectively. The transient distributions, corresponding to 1.3 kyr (E1) and 1.0 kyr (E3 and E4) after the start of the FFA, are those predicted at the time of minimum thermohaline overturning in the Atlantic. Contour intervals are 4 Sv and 10%. Regions where the water mass abundance is greater than 80% are shaded.

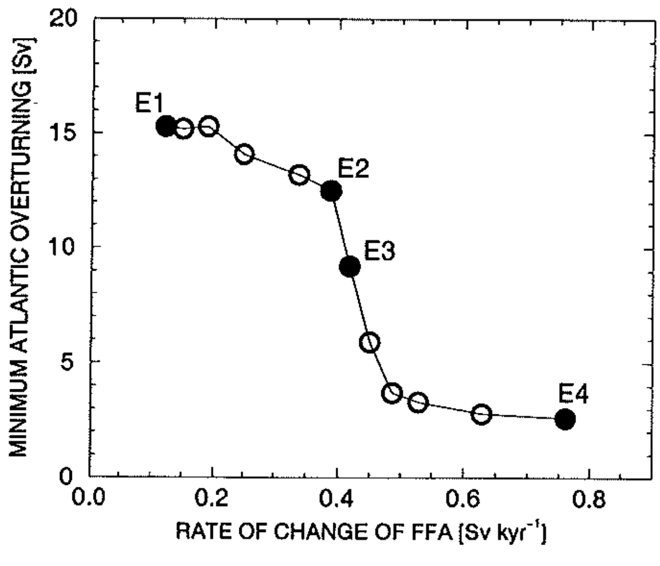

Figure 2. Minimum value of the maximum Atlantic stream function in 12 different experiments. The different experiments are characterized by the same volume of freshwater released ($6 \cdot 10^{15}$ m^3) and geographic application of the FFA (between 32.5°N–45°N in Atlantic), but by a different time rate of change of the FFA. Experiments labelled E1–E4 are examined here.

(dashed line in Fig. 4). Changes in the south are very small. On the other hand, the expected antiphasing is simulated whenever the THC shuts down completely (solid line in Fig. 4). The south exhibits a warming that is close in magnitude to the cooling in the north. Interestingly, our model simulations suggest that only complete shut-downs of the THC would be recorded in the South Atlantic and Southern Ocean.

3.2. $\Delta^{14}C$ Changes during Abrupt Events

Previous experiments with our model included radiocarbon as an inorganic tracer [*Stocker et al.*, 1992b; *Stocker and Wright*, 1996; *Stocker and Wright*, 1998]. We introduce here a more realistic treatment (Appendix) where ^{14}C is affected also by the ocean biological cycling (organic matter and $CaCO_3$ cycle). In the following we use the indexes "inorg" and "org" for $\Delta^{14}C$ to refer to the cases when ^{14}C is included as an inorganic and organic tracer, respectively.

We first consider the changes in global ocean export production in the three experiments examined below (E1, E3, and E4). These experiments are representative of, respectively, a small, intermediate, and strong reduction of the circulation in the North Atlantic (Fig. 2). We assume no isotope fractionation during $CaCO_3$ formation, so that $CaCO_3$ cycling does not directly affect the distribution of tracers here. The global ocean export production first decreases (by 5 to 20%, depending on the experiment) and then increases in each experiment (thin, dashed line in Fig. 5a–c). The changes in export production occur primarily in the North Atlantic where the development of the low-density freshwater cap inhibits the deepwater supply of PO_4 (Fig. 6a–b) and its subsequent erosion leads to a recharge of PO_4 in the euphotic zone (see also *Marchal et al.*, 1998b). We illustrate below the influence of changes in the ocean biological cycling on the atmospheric and oceanic $\Delta^{14}C_{org}$.

In each experiment the atmospheric $\Delta^{14}C_{org}$ first increases when the Atlantic thermohaline overturning is reduced and then decreases, essentially when the overturning resumes (solid line in Fig. 5a–c). This evolution is qualitatively similar to that in previous "inorganic" simulations with our zonally averaged model [*Stocker and Wright*, 1996; *Stocker and Wright*, 1998] and a three-dimensional ocean circulation model [*Mikolajewicz*, 1996]. The maximum positive anomaly in atmospheric ^{14}C activity is higher for a more drastic reduction of the THC, although $\Delta^{14}C_{org}$ reached in experiments E3 and E4 are quite comparable. In these two experiments the $\Delta^{14}C_{org}$ anomaly is initially slightly higher than the $\Delta^{14}C_{inorg}$ anomaly (short dashed line in Fig. 5b–c). This offset is due to a drop in the biological uptake of ^{14}C in the surface waters which varies in concert with the export production (Appendix). Subsequently, $\Delta^{14}C_{org}$ is lower than $\Delta^{14}C_{inorg}$ owing to the increasing ocean biological uptake. The maximum difference between the atmospheric $\Delta^{14}C_{inorg}$ and $\Delta^{14}C_{org}$ is equal to 7–8‰, depending on the experiment. This difference is small, but not neglibible compared to the anomalies of atmospheric $\Delta^{14}C_{inorg}$ and $\Delta^{14}C_{org}$ simulated in the individual experiments, which reach maxima of 20–35‰. We note that the initial increase in atmospheric $\Delta^{14}C_{inorg}$ and $\Delta^{14}C_{org}$ is consistent with the rise in atmospheric $\Delta^{14}C$ at the onset of the Younger Dryas documented in fossil coral and varved sediment records [*Edwards et al.*, 1993; *Goslar et al.*, 1995; *Björck et al.*, 1996; *Hughen et al.*, 1998; *Kitagawa and van der Plicht*, 1998; *Goslar et al.*, 1999]. Our simulations, however, do not exhibit a decrease in atmospheric $\Delta^{14}C$ during the model cold phase, in contrast to the gradual decline in atmospheric $\Delta^{14}C$ (corrected for changes in geomagnetic ^{14}C production) during the YD documented in the same records (see *Marchal et al.*, 1999). This decline remains a major problem to be solved in the future [*Goslar et al.*, 1999].

We now examine the distribution of $\Delta^{14}C_{org}$ in the three oceanic basins at the time of minimum Atlantic thermohaline overturning in experiments E1, E3, and

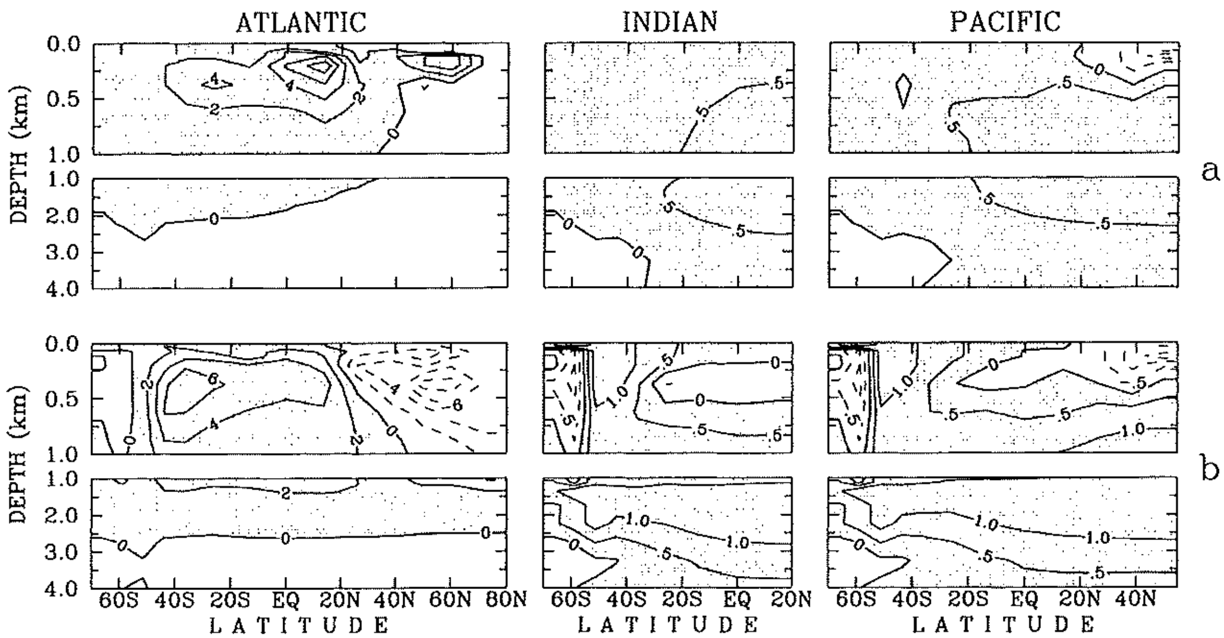

Figure 3. Latitude-depth distribution of the temperature anomaly (°C) simulated at the time of minimum Atlantic thermohaline overturning in experiments (a) E2, partial THC shut-down (0.8 kyr after start of FFA; THC drop from 24 Sv to 12 Sv) and (b) E4, complete shut-down (1.0 kyr after start of FFA; THC drop to 3 Sv). The contour interval is 2°C in the Atlantic and 0.5°C in the other basins. Regions with positive values are shaded.

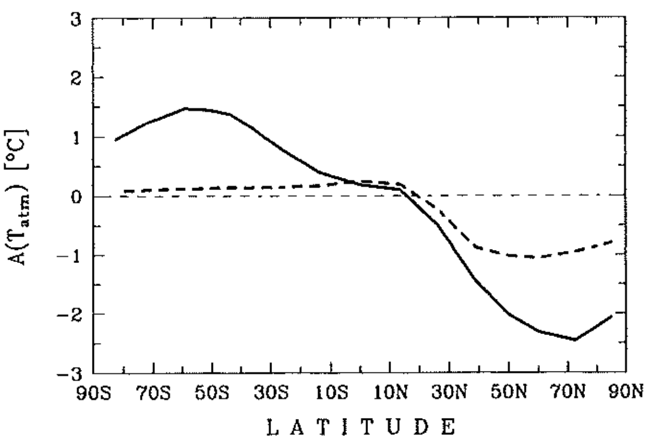

Figure 4. Meridional profile of the atmospheric temperature anomaly at the time of minimum THC in experiments E2 (– – –) and E4 (————).

E4 (Fig. 7b-d). $\Delta^{14}C_{org}$ exhibits an increase generally above ~ 2000 m in each basin, and a decrease at depth, essentially in the North Atlantic (Fig. 8a-c). Again, these results are in line with previous inorganic simulations with our model and a 3-d model [*Mikolajewicz*, 1996]. The maximum difference between the anomalies of oceanic $\Delta^{14}C_{inorg}$ and $\Delta^{14}C_{org}$ ranges from −9 to +7‰, depending on the ocean basin and the experiment. More than 99% of the variance of $\Delta^{14}C_{org}$ is explained by a linear regression against $\Delta^{14}C_{inorg}$ in E1, E3, and E4. Thus, changes in biological cycling have a minor effect on the oceanic $\Delta^{14}C_{org}$ anomalies simulated by our model and these anomalies can safely be interpreted as reflecting a local imbalance between air-sea gas exchange, oceanic transport, and radioactive decay.

The largest negative $\Delta^{14}C_{org}$ anomalies, amounting to about −100‰ in each experiment, are predicted in the deep North Atlantic (Fig. 8a-c). These are clearly related to the retreat of freshly formed North Atlantic Deep Water which is rich in ^{14}C (Fig. 1b and Fig. 7a). The advance of the deep component of Southern Ocean Water (Fig. 1c) is insufficient to compensate the effect of this retreat, because this component contains much less ^{14}C than the freshly formed NADW as it reaches the deep North Atlantic. On the other hand, the largest positive $\Delta^{14}C_{org}$ anomaly, greater than 60‰, is simulated in the upper kilometer of the South Atlantic in experiment E4 (Fig. 8c). Interestingly, the anomaly is coincident with the prominent subsurface warming predicted in this experiment (Fig. 3b). We infer that the ^{14}C enrichment and temperature increase are associated with the partial replacement of cold SOW by the

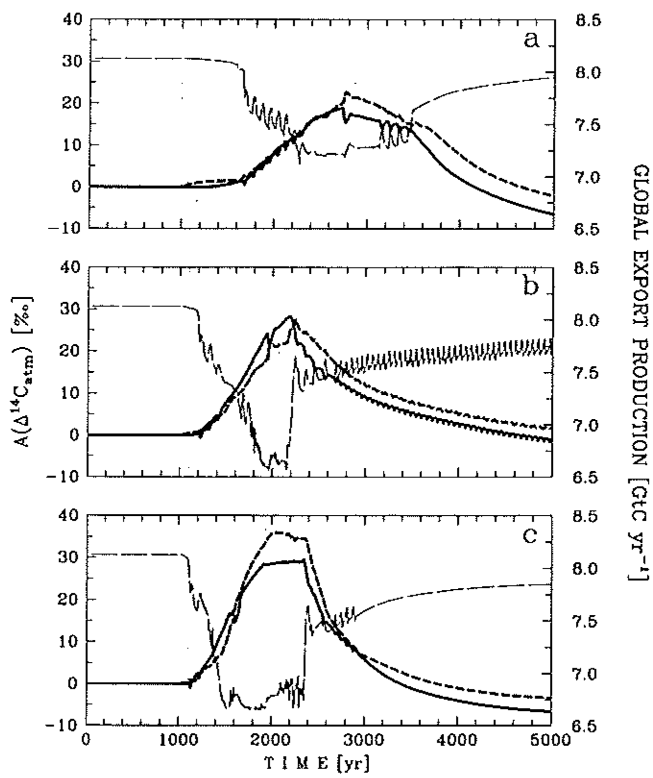

Figure 5. Atmospheric $\Delta^{14}C$ anomaly in experiments (a) E1, (b) E3, and (c) E4. The $\Delta^{14}C$ anomaly simulated when ^{14}C is included in the model as an inorganic tracer (– – –) and as an organic tracer (———) are represented. The global ocean export production (thin, dashed line) and the period during which the THC is altered (shaded area) are reported in each panel.

warmer Central Water (Fig. 1c–d), in a region where the convective activity and hence ^{14}C transport to depth is enhanced. Finally, we note that the positive $\Delta^{14}C_{org}$ anomalies simulated at intermediate depths (< 2000 m) in the Southern Ocean, Indian, and Pacific (Fig. 8a–c) cannot be due to $\Delta^{14}C_{org}$ changes occurring below since the former are negative. These anomalies evidence a far-field effect, whereby the reduction of deepwater formation in the North Atlantic produces an increase in the atmospheric ^{14}C activity which is then transmitted to the other basins through the sea surface by gas exchange.

3.3. Oceanic PO_4 and $\delta^{13}C$ Changes during Abrupt Events

The reduction of the Atlantic thermohaline overturning in the different experiments has a variable influence on the distribution of PO_4 and $\delta^{13}C$ in the ocean (Figs. 9 and 10). Negligible PO_4 and $\delta^{13}C$ anomalies at the depth of the NADW core in the model steady state are simulated in experiment E1 where the Atlantic thermohaline overturning is reduced to only ~ 15 Sv (Fig. 11a and 12a). By contrast, the anomalies become paleoceanographically significant when the overturning drops to 9 and 3 Sv (Fig. 11b–c and 12b–c). Strong PO_4 increases (> 0.3 mmol m^{-3}) and $\delta^{13}C$ decreases (< –0.3‰) are then present in the deep North Atlantic, with a general decline of their absolute amplitude from north to south in this basin. The chemical and isotopic shifts in the other basins, are much smaller, except for $\delta^{13}C$ at some locations in the South Indian, South Pacific, and Southern Ocean (Fig. 12b–c).

The oceanic PO_4 and $\delta^{13}C$ anomalies simulated in our experiments must be related to changes in the local rate of organic matter oxidation, air-sea gas exchange (affecting the preformed $\delta^{13}C$), and/or proportion of the deep water masses. We consider plots of $\delta^{13}C$ anomaly versus PO_4 anomaly predicted in the Atlantic and Southern Ocean in order to identify the most influential processes (Fig. 13). The general trend expected if these anomalies were caused only by organic matter cycling, is indicated by a solid line in each plot. This Redfield line has a negative slope of –1.2‰ (mmol m^{-3})$^{-1}$ based on model stoichiometry [*Marchal et al.*, 1998a]. Departures from this line, represented by dashed lines labeled with numbers expressed in ‰, reflect the effects of the air-sea gas exchange which influences $\delta^{13}C$, but not PO_4.

Two major features appear in the plots of $\delta^{13}C$ anomaly versus PO_4 anomaly (Fig. 13). First, waters deeper than 1000 m in the North Atlantic (ocean domain I below) exhibit strong PO_4 enrichment and $\delta^{13}C$ depletion. The departure from the Redfield line is less than +0.5‰ in each experiment (filled circles). Second, waters in the upper 1000 m in the Atlantic south of 65°N and in the Southern Ocean (domain II) exhibit a very strong $\delta^{13}C$ depletion with a moderate PO_4 decrease ("+" in Fig. 13). The departures from the Redfield line are larger for a greater reduction of the THC and reach more than 1‰ at some locations in experiments E3 and E4 (Fig. 13b–c). We note that $\delta^{13}C$ of waters in the upper 1000 m north of 65°N in the Atlantic (domain III) rises by more than 1‰ in experiment E4 (× in Fig. 13c). On the other hand, waters between 1–4 km in the South Atlantic and Southern Ocean (domain IV; open circles in Fig. 13) exhibit much lower chemical and isotopic shifts than in the same depth interval in the North Atlantic.

The first major feature in the $\delta^{13}C$ anomaly–PO_4 anomaly plots is examined with more detail. The small

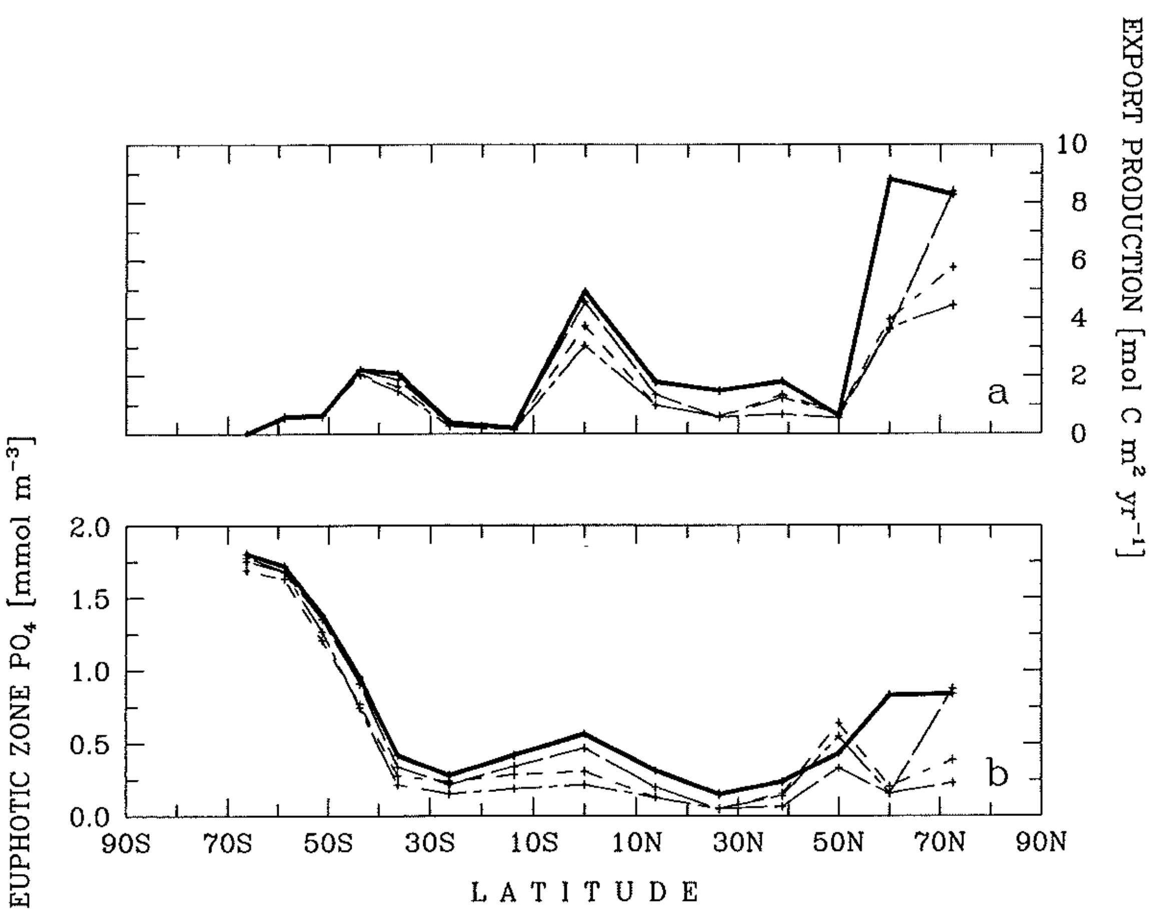

Figure 6. Meridional profile of (a) export production and (b) mean PO_4 concentration in the euphotic zone (top 100 m) in the Atlantic. The different curves correspond to the initial model steady state (———) and to the time of minimum THC in experiments E1 (—— —— ——), E3 (—— - ——), and E4 (– – –).

departure from the Redfield line indicates that the air-sea gas exchange has a relatively minor influence on the $\delta^{13}C$ anomalies and points to organic matter cycling as an important process. We identify whether the strong PO_4 and $\delta^{13}C$ anomalies simulated at the depth of the NADW core are related to an increase in the local rate of organic matter oxidation, Δ_{org}. This increase is calculated as:

$$\Delta_{org} = \int_{t_0}^{t_0+\Delta t} J_{org}(t)dt - J_{org}(t_0) \cdot \Delta t, \qquad (1)$$

where J_{org} is here the local rate of DIC production through the oxidation of POC and DOC_l, t_0 is the time of the initial steady state, and $t_0 + \Delta t$ is the time corresponding to the PO_4 and $\delta^{13}C$ anomalies, i.e. $\Delta t =$ 1.3 kyr in experiment E1 and 1.0 kyr in experiments E3 and E4. In experiments E3 and E4, Δ_{org} is negative in the North Atlantic (non shaded areas in Fig. 11b–c and 12b–c). This shift is due to the lowered injection of surface, DOC_l-rich waters to depth in the northern North Atlantic and, to a lesser extent, to the drop in the oxidation rate of POC associated with the decline in export production. Thus, the prominent chemical and isotopic changes predicted in the NADW core cannot result from an increase in the local rate of organic matter oxidation. These changes are related, instead, to a drop in the ventilation by PO_4-poor and $\delta^{13}C$-rich waters which becomes insufficient to balance the effects of organic matter oxidation at depth.

The second major feature in the $\delta^{13}C$ anomaly–PO_4 anomaly plots is the atypical $\delta^{13}C$ depletion in the upper 1000 m in the Atlantic south of 65°N and in the Southern Ocean. A possible effect here is a decrease in surface $\delta^{13}C$, associated with the decrease in export

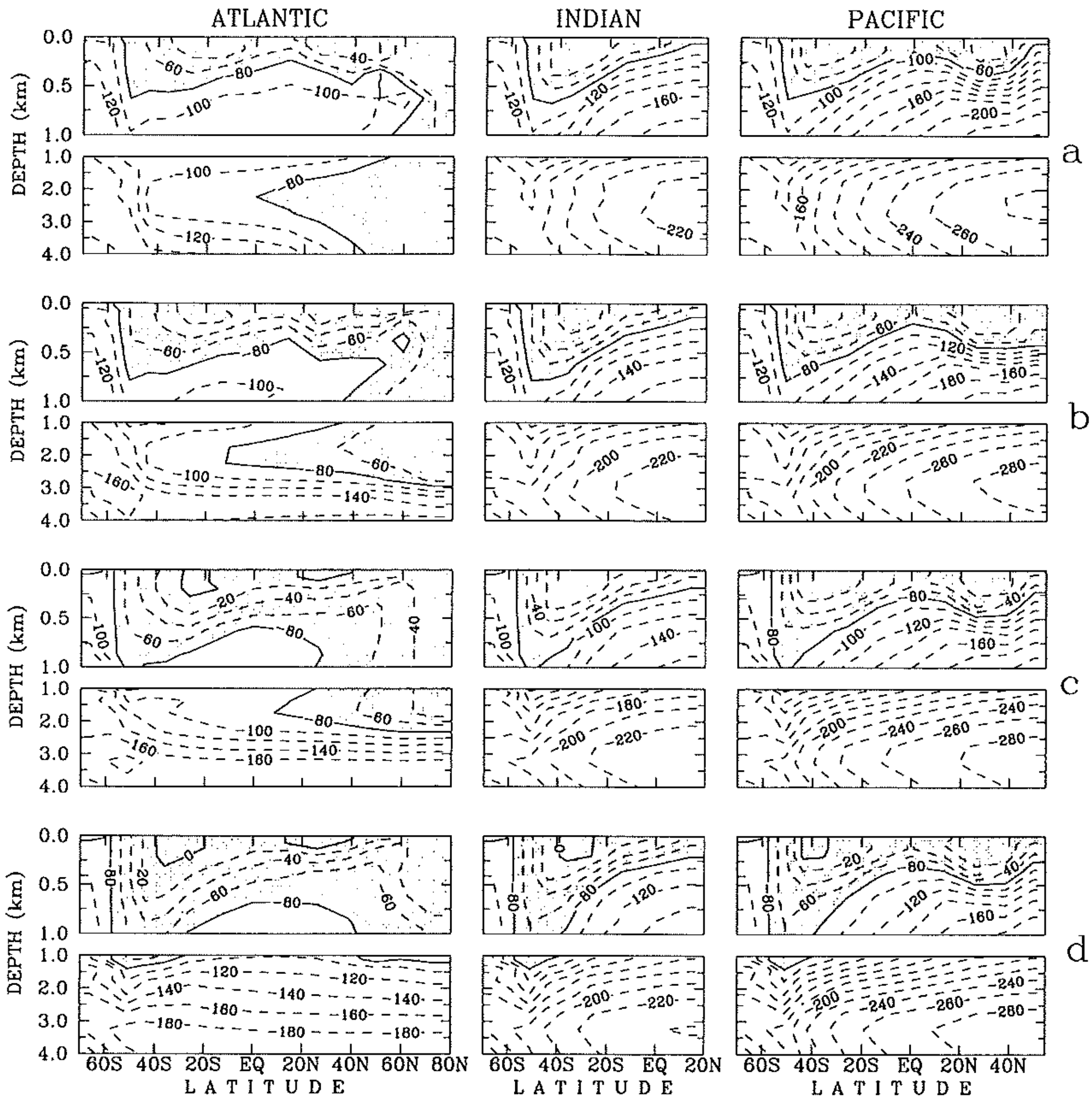

Figure 7. Latitude-depth distribution of $\Delta^{14}C$ (‰) simulated when ^{14}C is included as an organic tracer at the initial steady state (a) and at the time of minimum THC in experiments E1 (b), E3 (c), and E4 (d). The contour interval is 20‰. Regions where $\Delta^{14}C > -80$‰ are shaded.

production, which would occur in the absence of phosphate. Whereas the export production generally declines (Fig. 6a), the PO_4 level in the euphotic zone does not go to depletion in the Atlantic and Southern Ocean (Fig. 6b). This leads us to conclude that $\delta^{13}C$ of domain II-waters are markedly influenced by the effects of air-sea gas exchange. We now inspect the changes in the surface $\delta^{13}C$, $\delta^{13}C_{surf}$, and in the surface $\delta^{13}C$ expected from isotopic equilibrium with the atmosphere, $\delta^{13}C_{eq}$ (Fig. 14a–b). In the three experiments (E1, E3, and E4) the surface waters south of 30°N in the Atlantic become isotopically lighter. By contrast, the surface waters further north in the same basin exhibit generally an isotopic enrichment. $\delta^{13}C_{eq}$, on the other

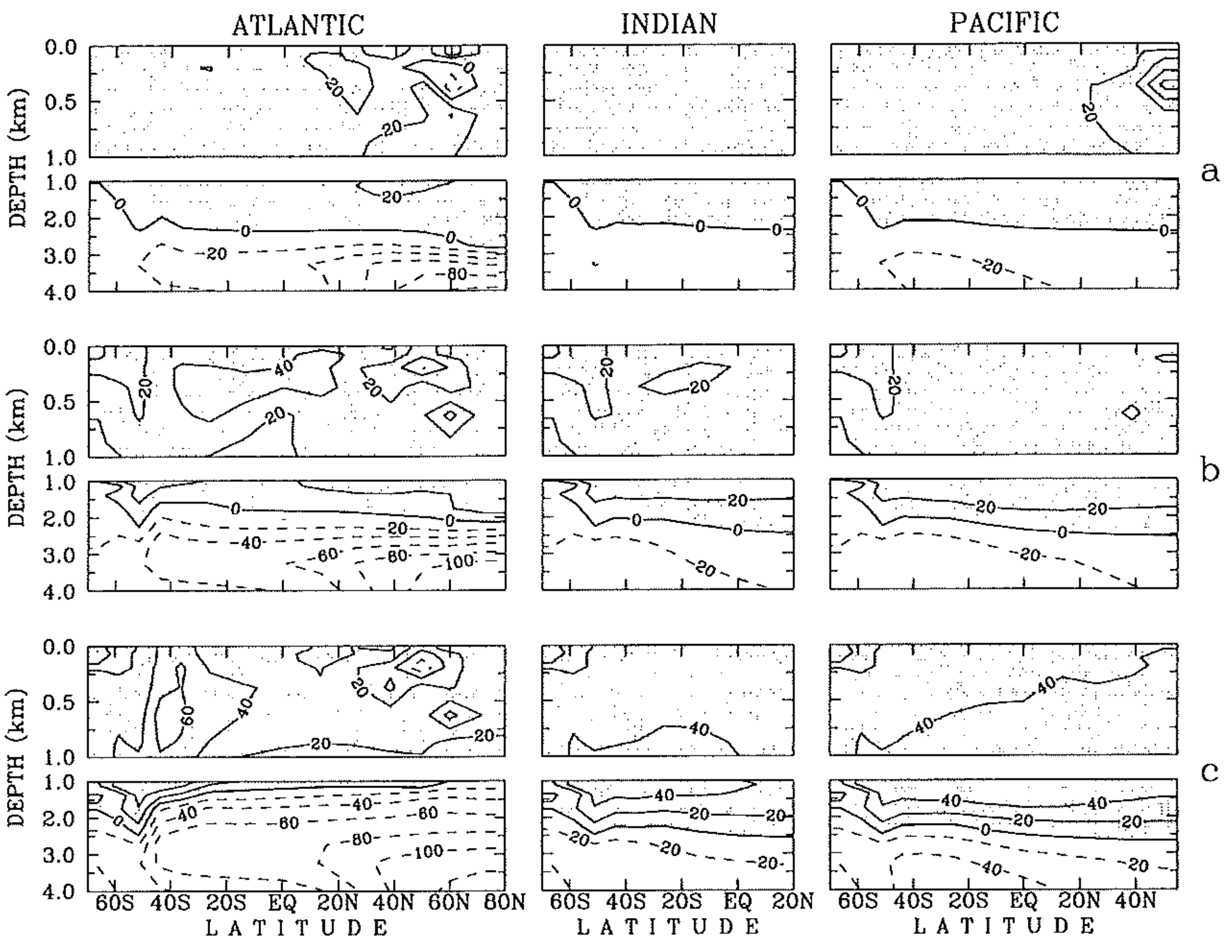

Figure 8. Latitude-depth distribution of $\Delta^{14}C$ anomaly (‰) with respect to the initial state (Fig. 7a) simulated when ^{14}C is included as an organic tracer at the time of minimum THC in experiments (a) E1, (b) E3, and (c) E4. The contour interval is 20‰. Regions with positive anomalies are shaded.

hand, is slightly depressed south of 30°N and enhanced north of this latitude. The fact that $\delta^{13}C_{surf}$ follow the $\delta^{13}C_{eq}$ changes suggests that the air-sea gas exchange is influential in producing the surface isotopic anomalies. More important, the absolute value of the isotopic disequilibrium, $\delta^{13}C_{surf} - \delta^{13}C_{eq}$, decreases generally at all latitudes in the Atlantic (Fig. 14c). A major contributor to this is likely the increasing residence time of waters at the surface in the Atlantic when the THC is partially (experiments E1 and E3) or completely collapsed (E4), which permits a better isotopic equilibration with the atmosphere. Interestingly, the isotopic anomalies are propagated to depth once they are generated at the surface (Fig. 9c–d and 10c–d). In the South Atlantic, this occurs through the deepening of the Central Water (Fig. 1d) which contains a small amount of PO_4 but is strongly depleted in $\delta^{13}C$. Thus, we infer that a combination between changes in the air-sea gas exchange and oceanic transport is responsible for the PO_4 and $\delta^{13}C$ anomalies simulated in the upper 1000 m of the Atlantic (Fig. 13b–c).

4. SUMMARY AND CONCLUSIONS

4.1. *Physical Changes*

It was initially proposed that variations in the flux of the relatively warm NADW would lead to a temperature evolution in phase in the two hemispheres [*Weyl*, 1968]. *Imbrie et al.* [1992] argued that this "NADW–Antarctic connection" contributed to the progression of climatic anomalies at Milankovitch frequencies from the Arctic to the other regions. *Bender et al.* [1994a] observed that

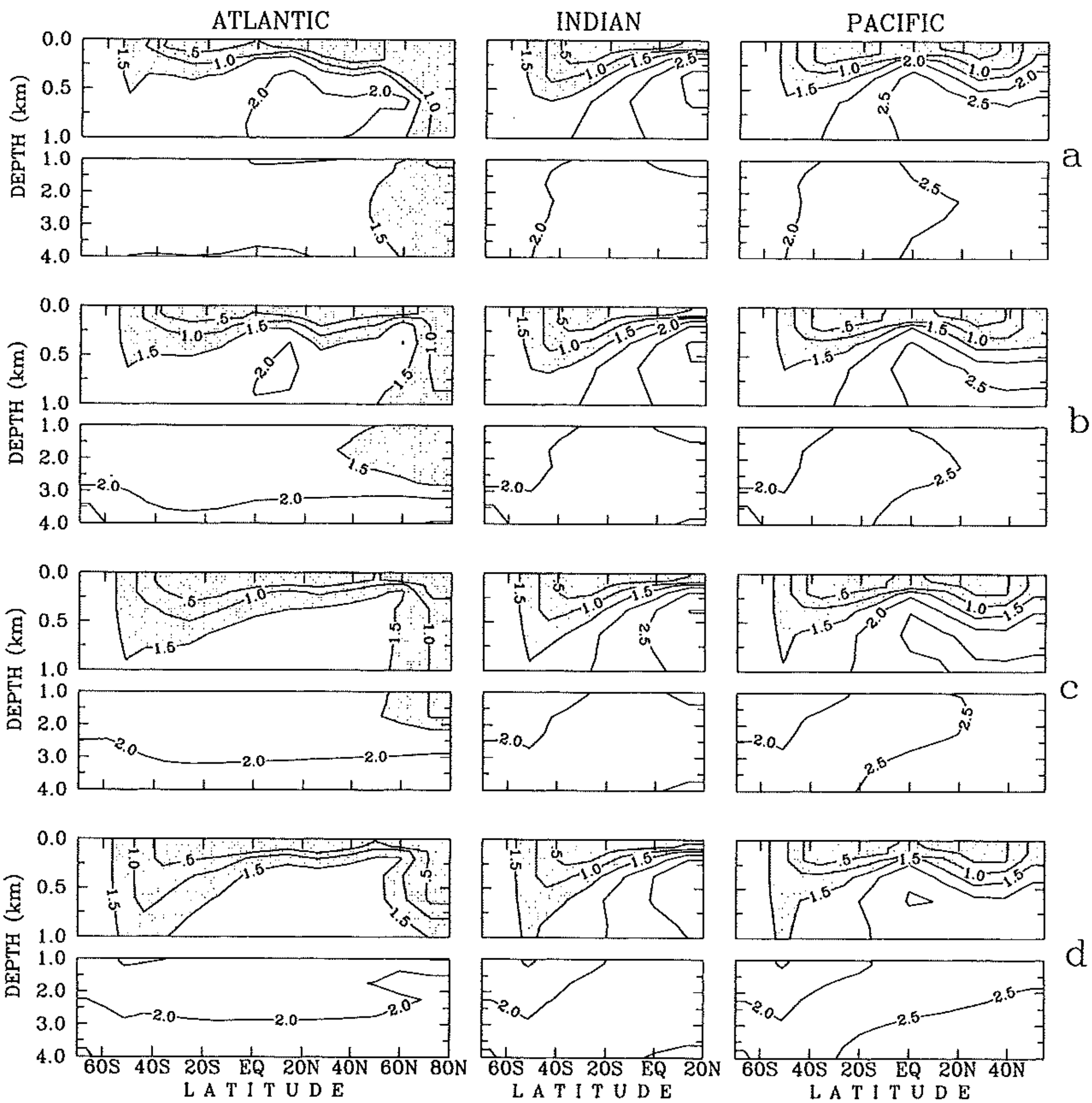

Figure 9. Latitude-depth distribution of PO_4 ($mmol\,m^{-3}$) at the initial steady state (a) and at the time of minimum THC in experiments E1 (b), E3 (c), and E4 (d). The contour interval is 0.5 $mmol\,m^{-3}$. Regions where $PO_4 < 1.5$ $mmol\,m^{-3}$ are shaded.

isotopic events are more rapid and more numerous in ice records from Greenland than from Antarctica. They inferred that long interstadials first originated in the northern hemisphere and were then transmitted to the other hemisphere. This would have occurred through partial deglaciation and changes in ocean circulation [*Bender et al.*, 1994a]. These authors cautioned, however, that their inference cannot be proven (past changes in the $^{18}O/^{16}O$ ratio of atmospheric O_2 are too small to permit a sufficently accurate synchronization of the ice cores).

The occurrence of a NADW–Antarctic connection at millennial time scale is not supported by the following lines of evidence. First, the CH_4-synchronization of ice core records from both polar regions implies that Greenland interstadials which occurred between 47–23 kyr BP lagged their isotopic counterparts at Byrd and Vostok by 1–2.5 kyr on average [*Blunier et al.*, 1998].

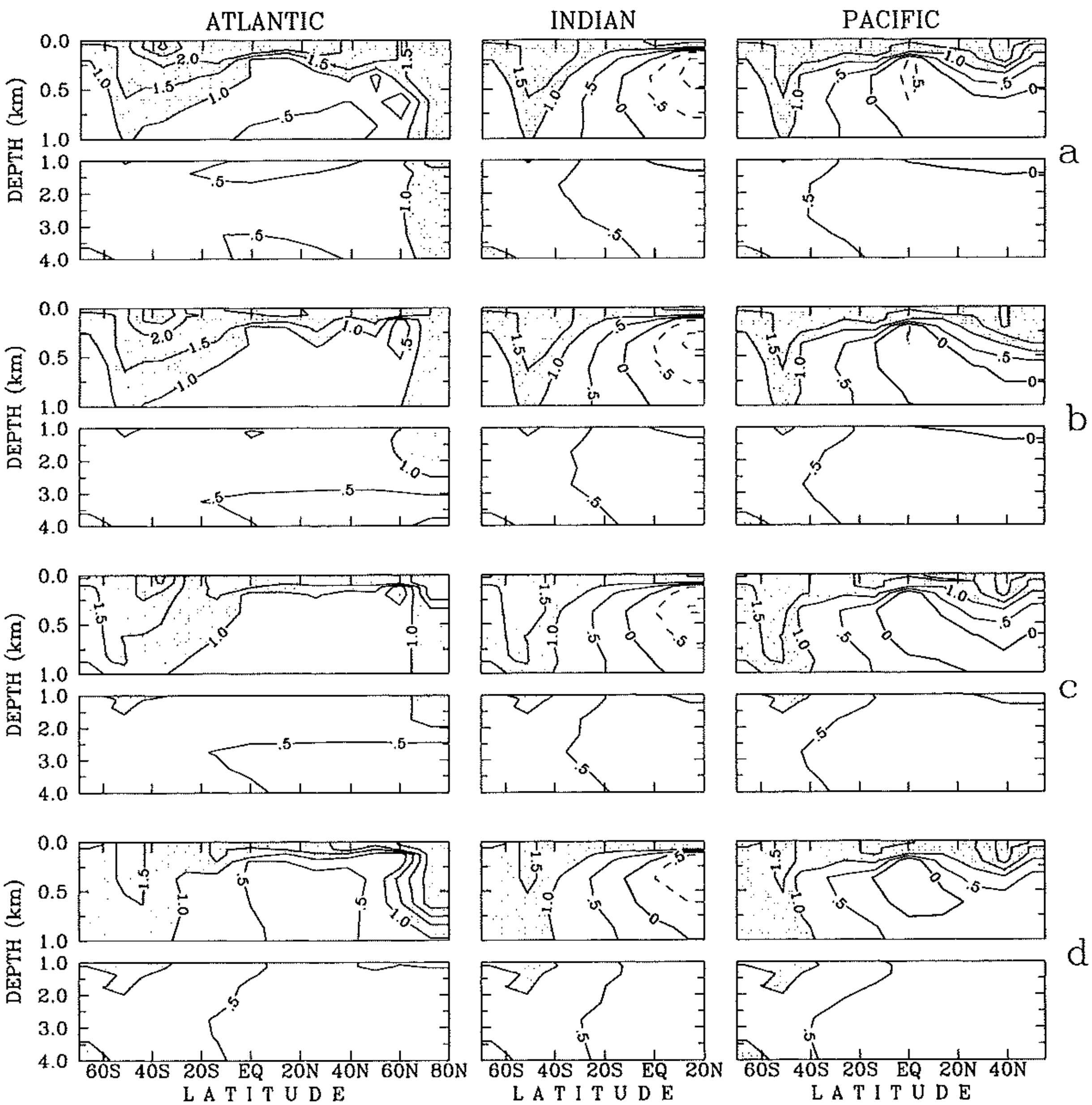

Figure 10. Latitude-depth distribution of $\delta^{13}C$ (‰) at the initial steady state (a) and at the time of minimum THC in experiments E1 (b), E3 (c), and E4 (d). The contour interval is 0.5 ‰. Regions where $\delta^{13}C > 1$ ‰ are shaded.

Second, in a high-resolution sediment core raised from the Southern Ocean, the planktonic $\delta^{18}O$ anomalies (a proxy of local SST) lead the benthic $\delta^{13}C$ anomalies (a proxy of deepwater production in the northern North Atlantic) by ~ 1,500 yr [*Charles et al.*, 1996]. Finally, the NADW–Antarctic connection is inconsistent with various model simulations which exhibit pronounced climate antiphasing between high northern and southern latitudes during periods where the THC is substantially altered [*Stocker*, 1999].

In our simplified model, freshwater-induced reductions of the Atlantic thermohaline circulation produce cooling at high northern latitudes and warming at high southern latitudes. Conversely, the resumption of the THC from a state of total collapse promotes warming in the north and cooling in the south. An interesting

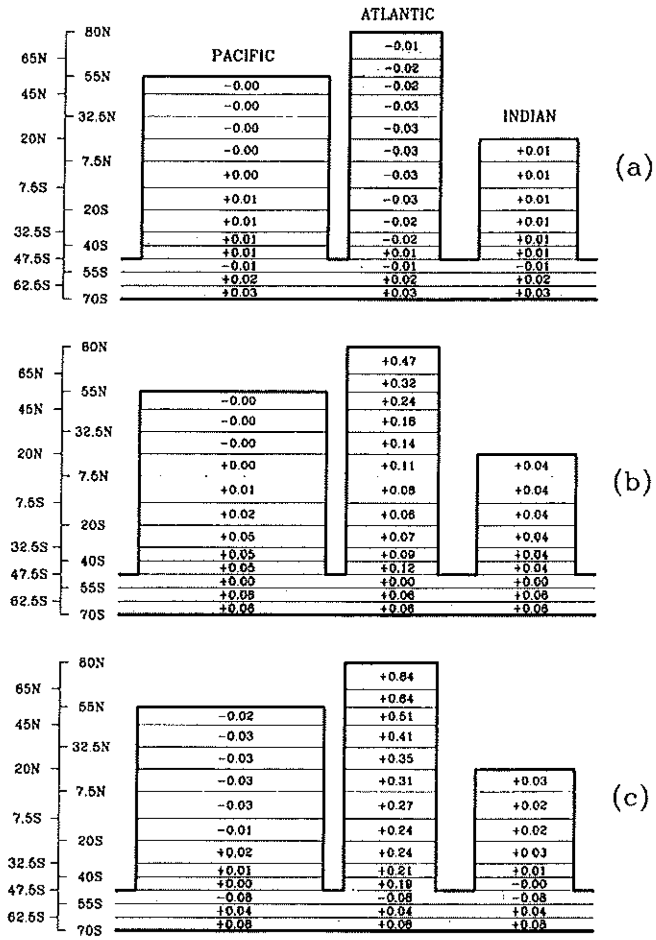

Figure 11. Distribution of the PO_4 anomaly (mmol m^{-3}) at the depth of 2250 m (corresponding to the core of the NADW in the initial model steady state) at the time of minimum THC in experiments E1 (a), E3 (b), and E4 (c). Regions where $\Delta_{org} > 0$ (see text for definition) are shaded.

hypothesis is that this mechanism has contributed, at least partly, to the north-south climatic antiphasing during the prominent Greenland interstadials 12, 8, 1 [*Blunier et al.*, 1998] and the Younger Dryas termination [*Blunier et al.*, 1997]. When these northern hemisphere warming events initiated (within several decades) the gradual warming that occurred previously in Antarctica was interrupted and followed either by a strong cooling, such as after the Greenland interstadials 12 and 8 [*Blunier et al.*, 1998], or a moderate cooling or a plateau such as the Antarctic Cold Reversal after interstadial 1 (Bølling/Allerød) and after the YD termination [*Jouzel et al.*, 1995; *Sowers and Bender*, 1995; *Blunier et al.*, 1997]. Recently, *Steig et al.* [1998] synchronized the δD record from Taylor Dome, a near-coastal East Antarctic site, to the GISP2 δD record based on measurements of the $^{18}O/^{16}O$ ratio of O_2 and of the CH_4 content in both cores. They documented that, unlike Byrd and Vostok, Taylor Dome experienced an abrupt warming at the onset of the Bølling and temperature minima during the YD in the Greenland record. A possible cause of the apparent inconsistency between the different Antarctic records is that short-term climate changes were not uniform throughout Antarctica.

Moreover, in our experiments, cooling in the north is less and not accompanied by temperature changes in the south in the case of partial collapses of the Atlantic thermohaline circulation. Another hypothesis is therefore that the shorter Greenland $\delta^{18}O$ oscillations do not have clear counterparts in isotopic records from

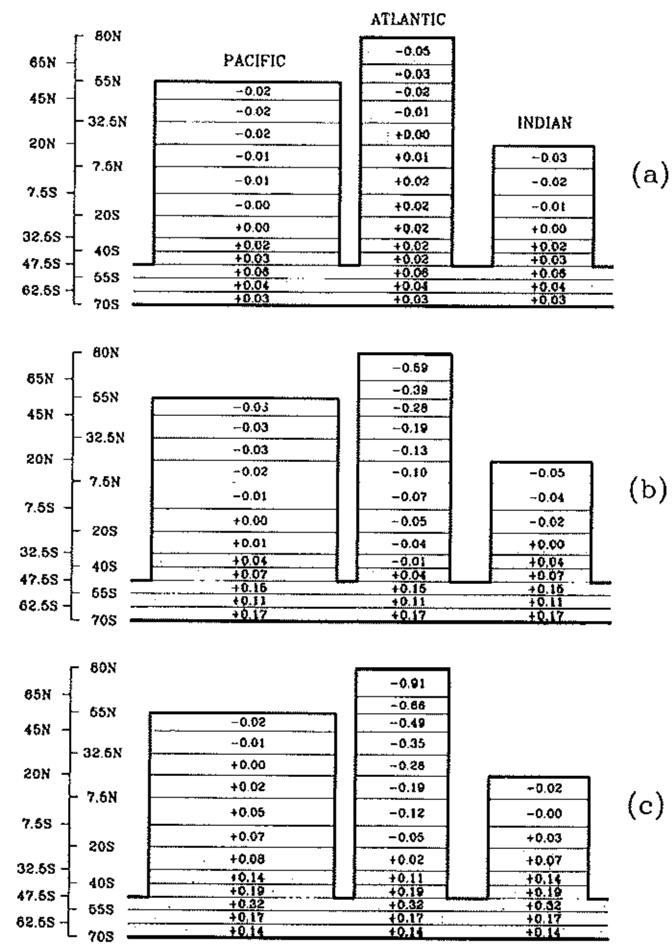

Figure 12. Distribution of the $\delta^{13}C$ anomaly (‰) at the depth of 2250 m (corresponding to the core of the NADW in the initial model steady state) at the time of minimum THC in experiments E1 (a), E3 (b), and E4 (c). Regions where $\Delta_{org} > 0$ (see text for definition) are shaded.

Byrd and Vostok [*Blunier et al.*, 1998] because the two hemispheres are decoupled in this case. Clearly, major questions remain regarding the millennial-scale climate changes of the last glacial period [*Stocker*, 1998; *Cane*, 1998].

First, we stress that we have examined only one potential mechanism with a particular model. On the one hand, a clear distinction must be made between the freshwater perturbation experiments done here and the more general issue of reducing the ocean thermohaline circulation. It is obvious that factors other than meltwater discharges in the North Atlantic basin and not included in our experiments could also alter the THC. For instance, simulations with a 3-d ocean circulation model illustrate that southern hemisphere climate could impact the northward inflow of warm waters into the North Atlantic and the southward ouflow from this basin through the westerly wind stress in the circumpolar region [*Toggweiler and Samuels*, 1993]. In addition, many processes which could have contributed to the fast climatic changes of the last glacial period are not represented. These processes include, for example, the feedback between the northward heat flux by the THC and glacial meltwater discharge at high northern latitudes, sea level changes affecting the stability of remote ice shelves, and variations in the atmospheric transport of water vapor. On the other hand, the

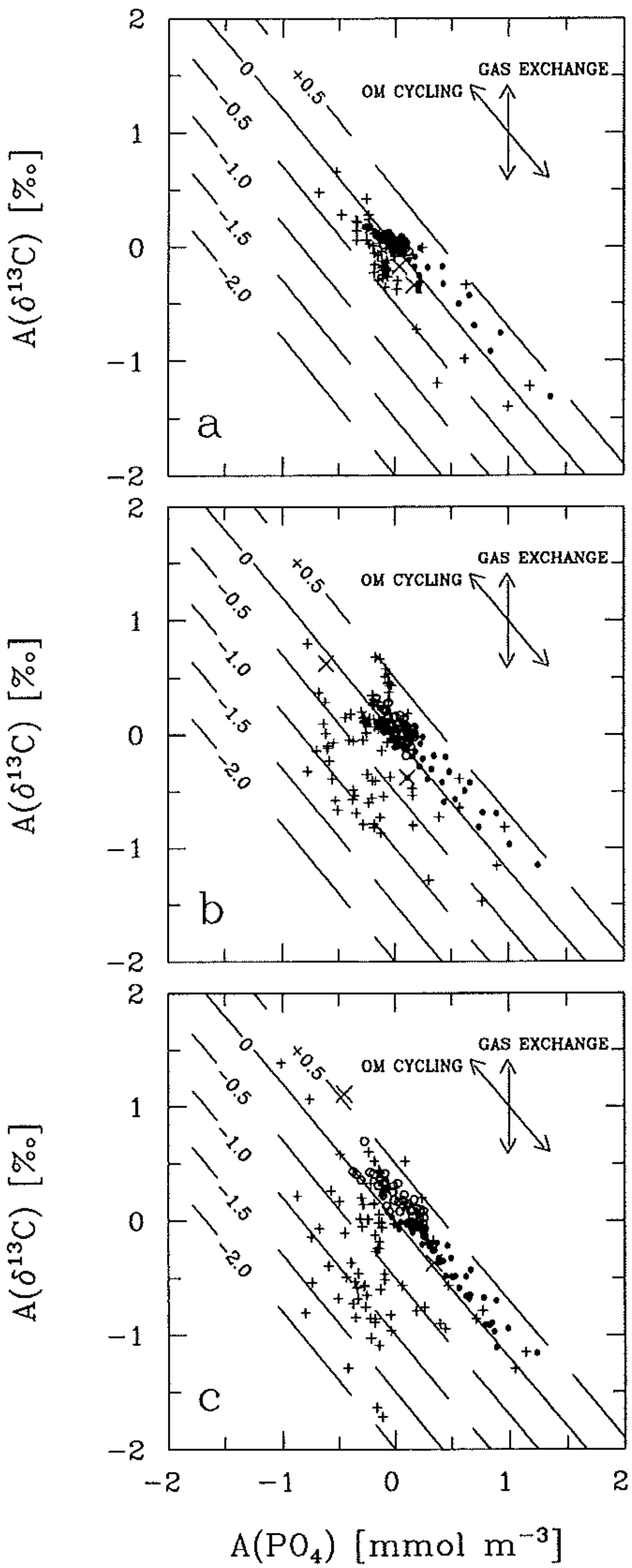

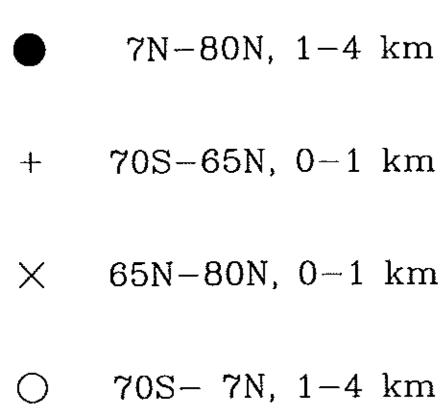

Figure 13. $\delta^{13}C$ anomaly versus PO_4 anomaly in four different domains in the Atlantic at the time of minimum THC in experiments E1 (a), E3 (b), and E4 (c). The solid line has a slope of -1.2 ‰ $(\mathrm{mmol\,m^{-3}})^{-1}$ and illustrates the composition change expected from the effect of organic matter cycling. The dashed lines represent various departures from this line and illustrate composition changes expected from the effect of air-sea gas exchange.

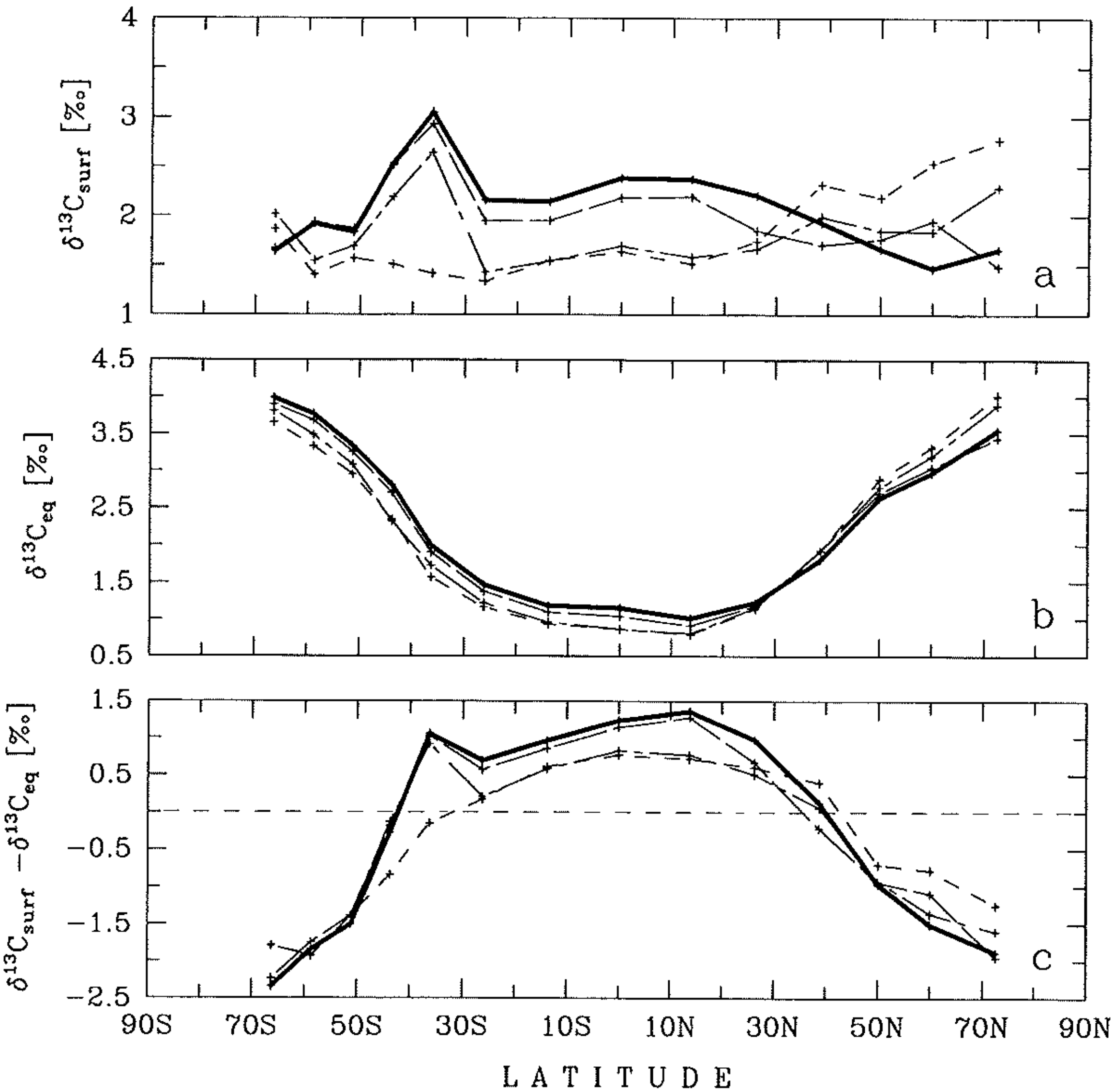

Figure 14. Meridional profile of (a) surface $\delta^{13}C$, $\delta^{13}C_{surf}$, (b) surface $\delta^{13}C$ expected from the equilibrium with the atmosphere, $\delta^{13}C_{eq}$, and (b) air-sea isotopic disequilibrium $\delta^{13}C_{surf} - \delta^{13}C_{eq}$. The different curves correspond to the initial model steady state (———) and to the time of minimum THC in experiments E1 (—— —— ——), E3 (—— - ——), and E4 (– – –).

limitations of our simplified model must be acknowledged. A major limitation comes from the zonal average representation of the ocean and atmosphere (for a discussion see *Wright and Stocker*, 1993). It is thus imperative that the scenario illustrated here be confirmed by more complete models in order to obtain a more detailed understanding of the north-south thermal antiphasing documented for abrupt changes during the last glacial period.

Another question concerns the geographical location and nature of the trigger(s) of the climatic sequences documented in paleoarchives from the northern and southern hemispheres. According to *Imbrie et al.* [1992], both theory and observation show that the initial response to orbital forcing must occur at high northern latitudes. Recent observations would suggest that millennial-scale climate changes originated rather in the southern hemisphere [*Charles et al.*, 1996; *Blunier*

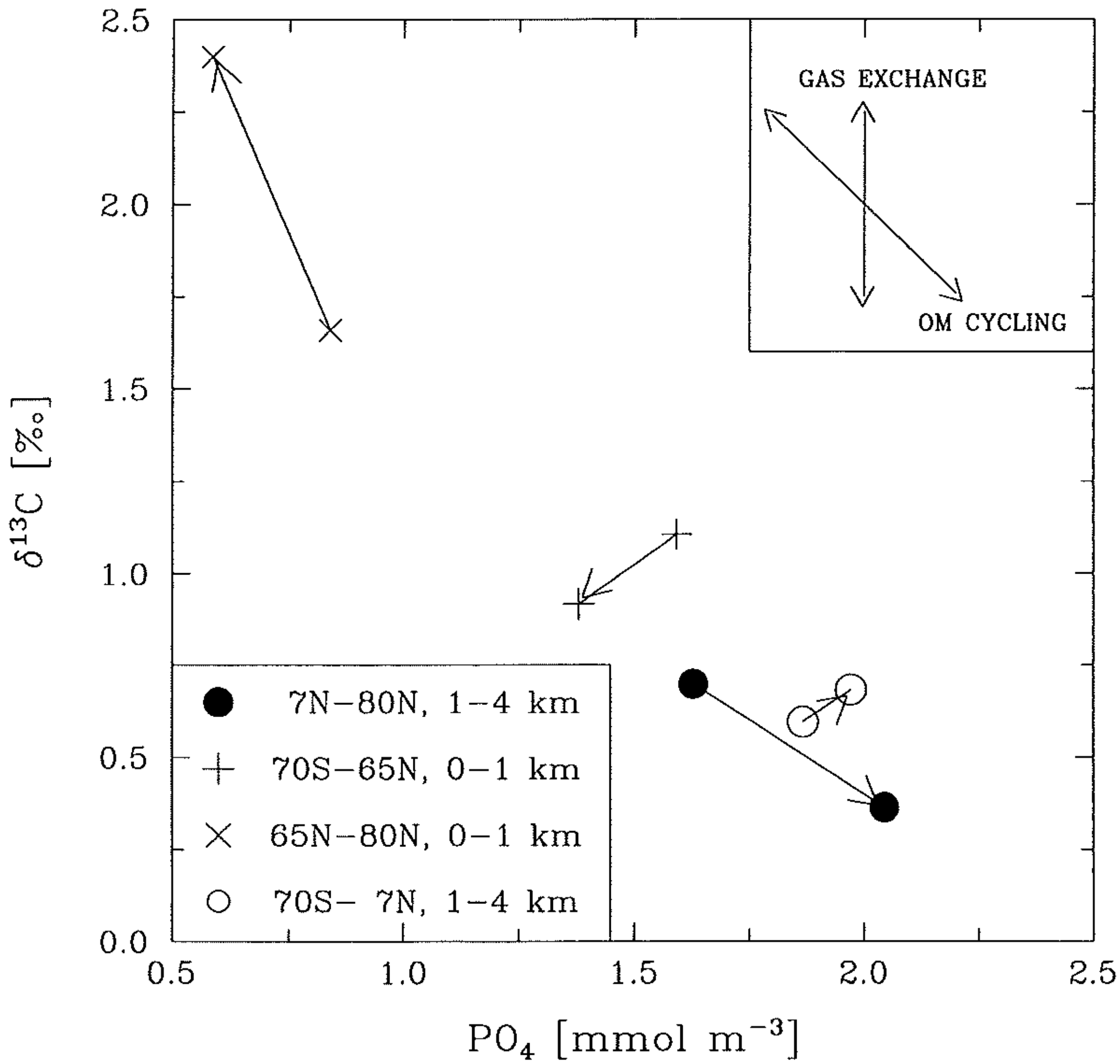

Figure 15. Volume-weighted mean $\delta^{13}C$ versus volume-weighted mean PO_4 in four different domains comprising the whole Atlantic basin (70°S–80°N) in experiment E4. The composition changes from the initial steady state to the time where the THC drops to a minimum of 3 Sv are illustrated by arrows. The composition changes expected from the effects of organic matter cycling and air-sea gas exchange are represented in the top right inset.

et al., 1998]. On the other hand, the role of the tropics and their interaction with middle and high latitudes need to be considered [*Chappellaz et al.*, 1993; *Guilderson et al.*, 1994; *McIntyre and Molfino*, 1996; *Bard et al.*, 1997; *Thompson et al.*, 1997]. The nature of interstadial forcing and response may well vary from one event to the next, as speculated by *Bender et al.* [1994a]. The search for cause-effect relations for millennial-scale climate changes is difficult much like for a mechanical system of two coupled oscillators in which the coupling constant can change in time.

4.2. Biogeochemical Changes

In addition to producing climate antiphasing between north and south, freshwater-induced changes of the THC also lead to spatially variable anomalies of $\Delta^{14}C$, PO_4, and $\delta^{13}C$ in our model. The simulated tracer anomalies are strongest when the THC collapses completely (experiment E4). In experiment E4, the average prominent PO_4 enrichment and $\delta^{13}C$ depletion between 1000 m in the North Atlantic (domain I) cannot only be due to mixing with a nutrient-rich end member, because the average composition of domain I-waters becomes extreme in the $\delta^{13}C$-PO_4 plot (filled circles in Fig. 15). The only mechanism to achieve this composition is through an imbalance between the remineralization of organic matter and the import of PO_4-poor and $\delta^{13}C$-rich waters. Interestingly, the averaged $\delta^{13}C$ depletion in domain I is less than that predicted by the Redfield line (see also Fig. 13c, which shows that domain I-waters are most generally shifted above this line). A likely contributor to this is the $\delta^{13}C$ enrichment of surface waters in the northern North Atlantic which are still transported to depth during the early phases of the THC collapse.

Waters in the upper 1000 m in the Atlantic south of 65°N and in the Southern Ocean (domain II; "+" in Fig. 15) experience, on average, moderate PO_4 and $\delta^{13}C$ depletions. The change in average composition is approximately orthogonal to that expected from organic matter cycling. This indicates that a combination between the air-sea gas exchange and oceanic transport is here influential. This is in line with our previous interpretation of the shift of domain II-waters to the bottom left quadrant in Fig. 13c.

Waters in the upper 1000 m north of 65°N in the Atlantic (domain III; × in Fig. 15) exhibit generally moderate PO_4 depletion but very strong $\delta^{13}C$ enrichment. Again, the change in average composition cannot be due to mixing with a PO_4-poor and $\delta^{13}C$-rich end member because the composition becomes extreme in the $\delta^{13}C$-PO_4 plot. The only possibility is therefore through a combination between surface gas exchange and organic matter cycling.

Finally, waters below 1000 m in South Atlantic and Southern Ocean (domain IV; open circles in Fig. 15) experience, on average, much smaller chemical and isotopic shifts than those in domains I-III. Here, the change in average composition is upward and to the right in the $\delta^{13}C$-PO_4 plot, which allows us to rule out a dominant effect from organic matter cycling. The slight PO_4 enrichment must be associated with mixing with waters of the deep North Atlantic (domain I) which become strongly nutrient-rich. The small $\delta^{13}C$ increase, on the other hand, must be due to mixing with waters above 1000 m (domain II) whose average $\delta^{13}C$, though it has decreased, remains higher than that in domain IV below.

Our model experiments suggest that the same ocean circulation change in the Atlantic can produce very distinct anomalies of $\Delta^{14}C$, PO_4, and $\delta^{13}C$ between different depths, latitudes, and basins. Some regions exhibit prominent, but opposite chemical and isotopic shifts, whereas others are weakly sensitive to THC changes. These results suggest that deep sea records of foraminiferal $\Delta^{14}C$, Cd/Ca, and $\delta^{13}C$ need not necessarily exhibit a uniform response throughout the deep ocean during abrupt climatic changes.

APPENDIX A: BIOGEOCHEMICAL PROCESSES IN THE EUPHOTIC ZONE ($z < z_{eup}$)

The biological cycling and air-sea gas exchange of ^{14}C are based on the theoretical expectation that, for photosynthesis and surface gas exchange, the fractionation factor for the ^{14}C–^{12}C pair should be the square of the fractionation factor for the ^{13}C–^{12}C pair [*Craig*, 1954]. We consider separately the formulation of biogeochemical processes in the euphotic zone, in the aphotic zone, and at the sea surface.

Dissolved inorganic radiocarbon, $DI^{14}C$, is biologically consumed in the euphotic zone (top 100 m) through the formation of organic matter and carbonate particles. The volumetric rates of $DI^{14}C$ removal through the formation of organic matter, $J_{org}^{DI^{14}C}$, and carbonate particles, $J_{car}^{DI^{14}C}$, are expressed as:

$$J_{org}^{DI^{14}C} = R_w \alpha_{org}^2 J_{org}, \tag{A1}$$

$$J_{car}^{DI^{14}C} = R_w \alpha_{car}^2 r_p J_{org}, \tag{A2}$$

where R_w is the $DI^{14}C/DIC$ ratio, α_{org} and α_{car} are the fractionation factors for the pair ^{13}C–^{12}C for photosynthesis and calcification, respectively, J_{org} is the rate of DIC removal through the formation of organic matter, and r_p is the production ratio, i.e. the ratio between the production of $CaCO_3$ to the production of organic carbon in the euphotic zone. In our model, α_{org} depends on the concentration of aqueous CO_2 [*Rau et al.*, 1989], $\alpha_{car} = 1$ [*Mook*, 1986], J_{org} is described as a function of the concentration of PO_4 through Michaelis-Menten kinetics, and r_p is related to temperature [*Drange*, 1994].

The labile dissolved organic radiocarbon, $DO^{14}C_l$, is biologically produced in the euphotic zone owing to the formation of organic matter:

$$\begin{aligned} J_{org}^{DO^{14}C_l} &= -\sigma \cdot J_{org}^{DI^{14}C} \\ &= -\sigma \cdot R_w \alpha_{org}^2 J_{org}, \end{aligned} \qquad \text{(A3)}$$

$$J_{car}^{DO^{14}C_l} = 0, \qquad \text{(A4)}$$

where $\sigma = 0.5$ is the fraction of organic carbon sequestred into DOC_l [*Marchal et al.*, 1998a].

APPENDIX B: BIOGEOCHEMICAL PROCESSES IN THE APHOTIC ZONE ($z > z_{eup}$)

$DI^{14}C$ is produced in the aphotic zone (below 100 m) through the remineralization of organic matter and the dissolution of carbonate particles. We denote by $J_{pom}^{DI^{14}C}$ the recycling of fast sinking particulate organic matter, and by $J_{dom}^{DI^{14}C}$ the recycling of labile dissolved organic matter. Thus,

$$\begin{aligned} J_{org}^{DI^{14}C} &= J_{pom}^{DI^{14}C} + J_{dom}^{DI^{14}C} \\ &= -\frac{\partial F_{pom}^{DI^{14}C}}{\partial z} + \kappa\, DO^{14}C_l, \end{aligned} \qquad \text{(B1)}$$

$$J_{car}^{DI^{14}C} = -\frac{\partial F_{car}^{DI^{14}C}}{\partial z}, \qquad \text{(B2)}$$

where $F_{pom}^{DI^{14}C}$ and $F_{car}^{DI^{14}C}$ are the fluxes of $DI^{14}C$ associated with fast-sinking POM and carbonate particles at a given depth in the water column, and κ is a first-order decay rate calculated so that the ocean inventory of DOC_l remains constant in the simulations [*Najjar et al.*, 1992].

$F_{pom}^{DI^{14}C}$ and $F_{car}^{DI^{14}C}$ depend on the fluxes of fast-sinking POM and $CaCO_3$ at the base of the euphotic zone:

$$\begin{aligned} F_{pom}^{DI^{14}C}(z) &= F_{pom}^{DI^{14}C}(z_{eup}) \cdot \left(\frac{z}{z_{eup}}\right)^{-\epsilon} \\ &= -(1-\sigma) \int_0^{z_{eup}} J_{org}^{DI^{14}C}\, dz \cdot \left(\frac{z}{z_{eup}}\right)^{-\epsilon}, \end{aligned} \qquad \text{(B3)}$$

$$\begin{aligned} F_{car}^{DI^{14}C}(z) &= F_{car}^{DI^{14}C}(z_{eup}) \cdot \left(e^{-(z-z_{eup})/L_{dis}}\right) \\ &= -\int_0^{z_{eup}} J_{car}^{DI^{14}C}\, dz \cdot \left(e^{-(z-z_{eup})/L_{dis}}\right), \end{aligned} \qquad \text{(B4)}$$

where $\epsilon = 0.858$ is the exponent in the fast sinking POM remineralization profile [*Bishop*, 1989] and $L_{dis} = 3000$ m is the length scale of the $CaCO_3$ dissolution profile [*Marchal et al.*, 1998a]. The fluxes $F_{pom}^{DI^{14}C}$ and $F_{car}^{DI^{14}C}$ at the ocean bottom are recycled in the deepest model layer as our model does not include sediment burial.

Finally, $DO^{14}C_l$ is oxidized in the aphotic zone according to

$$J_{org}^{DO^{14}C_l} = -\kappa\, DO^{14}C_l, \quad \text{and} \qquad \text{(B5)}$$

$$J_{car}^{DO^{14}C_l} = 0. \qquad \text{(B6)}$$

APPENDIX C: GAS EXCHANGE

The net flux of $^{14}CO_2$ from the ocean to the atmosphere, $F_{wa,n}^{^{14}CO_2}$, is expressed as:

$$F_{wa,n}^{^{14}CO_2} = R_w \alpha_{wa}^2 F_{wa}^{CO_2} - R_a \alpha_{aw}^2 F_{aw}^{CO_2}, \qquad \text{(C1)}$$

where $F_{wa}^{CO_2}$ and $F_{aw}^{CO_2}$ are the gross fluxes of CO_2 from the ocean to the atmosphere and from the atmosphere to the ocean, R_w and R_a are the $^{14}C/(^{12}C + {}^{13}C)$ ratios of surface DIC and atmospheric CO_2, and α_{wa} and α_{aw} are the fractionation factors for the pair ^{13}C–^{12}C for the air-sea gas exchange. In our model, $F_{wa}^{CO_2}$ and $F_{aw}^{CO_2}$ are related to the air-sea difference of the partial pressure of CO_2 via a constant transfer coefficient $\mu = 0.067$ mol m^{-2} yr^{-1} μatm^{-1}, whereas α_{aw} and α_{wa} depend on temperature and DIC speciation in the surface water [*Marchal et al.*, 1998a].

We introduce appropriate scalings in the formulation of $F_{wa,n}^{^{14}CO_2}$ in the case where ^{14}C is included as an inorganic tracer, in order to compare consistently $\Delta^{14}C_{org}$ with $\Delta^{14}C_{inorg}$. The formulation of *Stocker and Wright* [1996] is used:

$$F_{wa,n}^{^{14}CO_2} = g\alpha_{wa}^2 \xi [DI^{14}C] - g\alpha_{aw}^2 [^{14}CO_2]_a^* \qquad \text{(C2)}$$

where g is the gas transfer velocity for CO_2, ξ is the buffer factor for $^{14}CO_2$ in seawater, and $[^{14}CO_2]^*_a$ is the concentration of atmospheric $^{14}CO_2$ in units of oceanic concentration. g is related to the CO_2 transfer coefficient μ through $g = \mu \cdot pCO^\circ_{2,w}/[DIC]^\circ$, where $pCO^\circ_{2,w}$ and $[DIC]^\circ$ are reference values of the partial pressure of CO_2 and DIC concentration in surface seawater, respectively. With $\mu = 0.067$ mol m^{-2} yr^{-1} μatm^{-1}, $pCO^\circ_{2,w}$ = 280 μatm, and $[DIC]^\circ = 2.052$ mol m^{-3}, we obtain $g = 9.1$ m yr^{-1}. We choose $\xi = 1$, which is a good approximation for $^{14}CO_2$ in seawater. Finally, $[^{14}CO_2]^*_a$ is calculated as $[^{14}CO_2]^*_a = [^{14}CO_2]_a \cdot \overline{[DIC]}^\circ / [CO_2]^\circ_a$, where $[^{14}CO_2]_a$ is the concentration of $^{14}CO_2$ in the atmosphere (mol m^{-3} of air), $\overline{[DIC]}^\circ = 2.250$ mol m^{-3} is a reference, ocean mean concentration of DIC, and $[CO_2]^\circ_a = 1.184 \cdot 10^{-2}$ mol m^{-3} is a reference concentration of atmospheric CO_2.

The concentrations of radiocarbon in the ocean and in the atmosphere are expressed in conventional $\Delta^{14}C$ units. In the organic case, $\Delta^{14}C$ is calculated as

$$\Delta^{14}C = (\frac{r_N}{r_{St}} - 1) \cdot 1000. \qquad (C3)$$

$r_{St} = 1.176 \cdot 10^{-12}$ is the standard $^{14}C/^{12}C$ ratio and r_N is the ^{13}C-normalized activity given by

$$r_N = r\left(1 - \frac{2(\delta^{13}C + 25\,‰)}{1000\,‰}\right), \qquad (C4)$$

where r is the $^{14}C/^{12}C$ ratio and $\delta^{13}C$ denotes the reduced isotopic ratio referenced to the PDB standard [*Craig*, 1957].

In the inorganic case, we omit isotopic fractionation during the gas exchange, i.e. $\alpha^2_{wa} = \alpha^2_{aw} = 1$. Thus, $\Delta^{14}C$ is calculated without the correction for isotopic fractionation. For the atmosphere:

$$\Delta^{14}C = \left(\frac{[^{14}CO_2]/[CO_2]^\circ_a}{r_{St}} - 1\right) \cdot 1000\,‰. \qquad (C5)$$

For the ocean:

$$\Delta^{14}C = \left(\frac{[DI^{14}C]/\overline{[DIC]}^\circ}{r_{St}} - 1\right) \cdot 1000\,‰. \qquad (C6)$$

Acknowledgments. J. R. Toggweiler and an anonymous reviewer provided useful comments. TS would like to thank P. Clark and R. Webb for a very stimulating Chapman Conference and the editorial efforts in completing this volume. This study was made possible by the Swiss National Science Foundation and the Swiss Federal Office of Science and Education through the European Projects ENV4-CT95-0131 "Variability of the Glacial and Interglacial Climates and Abrupt Climatic Changes" and ENV4-CT95-0130 "North-South Climatic Connection and Carbon Cycle over the last 250 kyr".

REFERENCES

Adkins, J. F., and E. A. Boyle, Changing atmospheric $\Delta^{14}C$ and the record of deep water paleoventilation ages, *Paleoceanography, 12*, 337–344, 1997.

Alley, R. B., D. A. Meese, C. A. Shuman, A. J. Gow, K. C. Taylor, P. M. Grootes, J. W. C. White, M. Ram, E. D. Waddington, P. A. Mayewski, and G. A. Zielinski, Abrupt increase in Greenland snow accumulation at the end of the Younger Dryas event, *Nature, 362*, 527–529, 1993.

Bard, E., M. Arnold, J. Mangerud, M. Paterne, L. Labeyrie, J. Duprat, M.-A. Mélières, E. Sønstegaard, and J.-C. Duplessy, The North Atlantic atmosphere-sea surface ^{14}C gradient during the Younger Dryas climatic event, *Earth Planet. Sci. Lett., 126*, 275–287, 1994.

Bard, E., F. Rostek, and C. Sonzogni, Interhemispheric synchrony of the last deglaciation inferred from alkenone paleothermometry, *Nature, 385*, 707–710, 1997.

Bender, M., T. Sowers, M.-L. Dickson, J. Orchardo, P. Grootes, P. A. Mayewski, and D. A. Meese, Climate correlations between Greenland and Antarctica during the past 100'000 years, *Nature, 372*, 663–666, 1994a.

Bender, M., T. Sowers, and L. Labeyrie, The Dole effect and its variations during the last 130,000 years as measured in the Vostok ice core, *Global. Biogeochem. Cycles, 8*, 363–376, 1994b.

Bishop, J. K. B., Regional extremes in particulate matter composition and flux: effects on the chemistry of the ocean interior, in *Productivity of the Ocean: Present and Past*, edited by W. H. Berger, V. S. Smetacek, and G. Wefer, pp. 117–137, John Wiley, New-York, 1989.

Björck, S., B. Kromer, S. Johnsen, O. Bennike, D. Hammarlund, G. Lemdahl, G. Possnert, T. L. Rasmussen, B. Wohlfahrt, C. U. Hammer, and M. Spurk, Synchronised terrestrial-atmospheric deglacial records around the North Atlantic, *Science, 274*, 1155–1160, 1996.

Blunier, T., J. Chappellaz, J. Schwander, A. Dällenbach, B. Stauffer, T. F. Stocker, D. Raynaud, J. Jouzel, H. B. Clausen, C. U. Hammer, and S. J. Johnsen, Asynchrony of Antarctic and Greenland climate change during the last glacial period, *Nature, 394*, 739-743, 1998.

Blunier, T., J. Schwander, B. Stauffer, T. Stocker, A. Dällenbach, A. Indermühle, J. Tschumi, J. Chappellaz, D. Raynaud, and J.-M. Barnola, Timing of temperature variations during the last deglaciation in Antarctica and the atmospheric CO_2 increase with respect to the Younger Dryas event, *Geophys. Res. Let., 24*, 2683-2686, 1997.

Boyle, E. A., Last-Glacial-Maximum North Atlantic Deep Water: on, off or somewhere in-between ?, *Phil. Trans. Roy. Soc., London, 348*, 243–253, 1995.

Boyle, E. A., and L. D. Keigwin, North Atlantic thermohaline circulation during the past 20,000 years linked to high-latitude surface temperature, *Nature, 330*, 35–40, 1987.

Broecker, W. S., D. Peteet, and D. Rind, Does the ocean-atmosphere system have more than one stable mode of operation ?, *Nature, 315*, 21–25, 1985.

Brook, E. J., T. Sowers, and J. Orchardo, Rapid variations in atmospheric methane concentration during the past 110,000 years, *Science, 273*, 1087–1091, 1996.

Cane, M. A., A role of the tropical Pacific, *Science, 282*, 59–61, 1998.

Chappellaz, J., T. Blunier, D. Raynaud, J. M. Barnola, J. Schwander, and B. Stauffer, Synchronous changes in atmospheric CH_4 and Greenland climate between 40 and 8 kyr BP, *Nature, 366*, 443–445, 1993.

Charles, C., and R. G. Fairbanks, Evidence from Southern Ocean sediments for the effect of North Atlantic deep-water flux on climate, *Nature, 355*, 416–419, 1992.

Charles, C. D., J. Lynch-Stieglitz, U. S. Ninnemann, and R. G. Fairbanks, Climate connections between the hemisphere revealed by deep sea sediment core/ice core correlations, *Earth Planet. Sci. Lett., 142*, 19–27, 1996.

Craig, H., Carbon 13 in plants and the relationship between carbon 13 and carbon 14 variations in nature, *J. Geol. 62*, 115–149, 1954.

Craig, H., Isotopic standards for carbon and oxygen and correction factors for mass-spectrometric analysis of carbon dioxide, *Geochim. Cosmochim. Acta, 12*, 133–149, 1957.

Crowley, T. J., North Atlantic deep water cools the southern hemisphere, *Paleoceanography, 7*, 489–497, 1992.

Cuffey, K. M., and G. D. Clow, Temperature, accumulation, and ice sheet elevation in central Greenland through the last deglacial transition, *J. Geophys. Res., 102*, 26383–26396, 1997.

Dansgaard, W., H. B. Clausen, N. Gundestrup, C. U. Hammer, S. F. Johnsen, P. M. Kristinsdottir, and N. Reeh, A new Greenland deep ice core, *Science, 218*, 1273–1277, 1982.

Dansgaard, W., S. J. Johnsen, H. B. Clausen, D. Dahl-Jensen, N. S. Gundestrup, C. U. Hammer, C. S. Hvidberg, J. P. Steffensen, A. E. Sveinbjornsdottir, J. Jouzel, and G. Bond, Evidence for general instability of past climate from a 250-kyr ice-core record, *Nature, 364*, 218–220, 1993.

Denton, G. H., and C. H. Hendy, Younger Dryas age advance of Franz Josef glacier in the southern alps of New Zealand, *Science, 264*, 1434–1437, 1994.

Drange, H., An isopycnic coordinate carbon cycle model for the North Atlantic; and the possibility of disposing of fossil fuel CO_2 in the ocean, Ph. D. thesis, 286 pp., Department of Mathematics, University of Bergen, Norway, 1994.

Edwards, R. L., W. J. Beck, G. S. Burr, D. J. Donahue, J. M. A. Chappell, A. L. Bloom, E. R. M. Druffel, and F. W. Taylor, A large drop in atmospheric $^{14}C/^{12}C$ and reduced melting in the Younger Dryas, documented with ^{230}Th ages of corals, *Science, 260*, 962–968, 1993.

Fanning, A. F., and A. J. Weaver, Temporal-geographical meltwater influences on the North Atlantic conveyor: Implications for the Younger Dryas, *Paleoceanography, 12*, 307–320, 1997.

Goslar, T., M. Arnold, E. Bard, T. Kuc, M. F. Pazdur, M. Ralska-Jasiewiczowa, K. Różański, N. Tisnerat, A. Walanus, B. Wicik, and K. Więckowski, High concentration of atmospheric ^{14}C during the Younger Dryas cold episode, *Nature, 377*, 414–417, 1995.

Goslar, T., B. Wohlfarth, S. Björck, G. Possnert, and J. Björck, Variations of atmospheric ^{14}C concentrations over the Allerød-Younger Dryas transition, *Clim. Dyn., 15*, 29–42, 1999.

Guilderson, T. P., R. G. Fairbanks, and J. L. Rubenstone, Tropical temperature variations since 20,000 years ago: Modulating interhemispheric climate change, *Science, 263*, 663–665, 1994.

Hughen, K. A., J. T. Overpeck, S. J. Lehman, M. Kashgarian, J. Southon, L. C. Peterson, R. Alley, and D. M. Sigman, Deglacial changes in ocean circulation from an extended radiocarbon calibration, *Nature, 391*, 65–68, 1998.

Imbrie, J., et al., On the structure and origin of major glaciation cycles, 1. Linear responses to Milankovitch forcing, *Paleoceanography, 7*, 701–738, 1992.

Jansen, E., and T. Veum, Evidence for two-step deglaciation and its impact on North Atlantic deep-water circulation, *Nature, 343*, 612–616, 1990.

Johnsen, S. J., H. B. Clausen, W. Dansgaard, K. Fuhrer, N. Gundestrup, C. U. Hammer, P. Iversen, J. Jouzel, B. Stauffer, and J. P. Steffensen, Irregular glacial interstadials recorded in a new Greenland ice core, *Nature, 359*, 311–313, 1992.

Johnsen, S. J., D. Dahl-Jensen, W. Dansgaard, and N. Gundestrup, Greenland palaeotemperatures derived from GRIP bore hole temperature and ice core isotope profiles, *Tellus, Ser. B, 47*, 624–629, 1995.

Jouzel, J., R. Vaikmae, J. R. Petit, M. Martin, Y. Duclos, M. Stievenard, C. Lorius, M. Toots, M. A. Mélières, L. H. Burckle, N. I. Barkov, and V. M. Kotlyakov, The two-step shape and timing of the last deglaciation in Antarctica, *Clim. Dyn., 11*, 151–161, 1995.

Keigwin, L. D., G. A. Jones, and S. J. Lehman, Deglacial meltwater discharge, North Atlantic deep circulation and abrupt climate change, *J. Geophys. Res., 96*, 16811–16826, 1991.

Keigwin, L. D., and S. J. Lehman, Deep circulation change linked to Heinrich event 1 and Younger Dryas in a mid-depth North Atlantic core, *Paleoceanography, 9*, 185–194, 1994.

Kitagawa, H., and J. van der Plicht, Atmospheric radiocarbon calibration to 45,000 yr BP: Late glacial fluctuations and cosmogenic isotope production, *Science, 279*, 1187–1190, 1998.

Lowell, T. V., C. J. Heusser, B. G. Anderson, P. I. Moreno, A. Hauser, L. E. Heusser, C. Schlüchter, D. R. Marchant, and G. H. Denton, Interhemispheric correlation of Late Pleistocene glacial events, *Science, 269*, 1541–1549, 1995.

Mabin, M. C. G., The age of the Waiho Loop glacial event, *Science, 271*, 668, 1996.

Manabe, S., and R. J. Stouffer, Simulation of abrupt climate change induced by freshwater input to the North Atlantic Ocean, *Nature, 378*, 165–167, 1995.

Manabe, S., and R. J. Stouffer, Coupled ocean-atmosphere model response to freshwater input: Comparison to

Younger Dryas event, *Paleoceanography, 12*, 321–336, 1997.

Marchal, O., T. F. Stocker, and F. Joos, A latitude-depth, circulation-biogeochemical ocean model for paleoclimate studies. Development and sensitivities, *Tellus, Ser. B, 50*, 290–316, 1998a.

Marchal, O., T. F. Stocker, and F. Joos, Impact of oceanic reorganizations on the ocean carbon cycle and atmospheric carbon dioxide content, *Paleoceanography, 13*, 225–244, 1998b.

Marchal, O., T. F. Stocker, F. Joos, A. Indermühle, T. Blunier, and T. Tschumi, Modelling the concentration of atmospheric CO_2 during the Younger Dryas climate event, *Clim. Dyn., 15*, 341–354, 1999.

McIntyre, A., and B. Molfino, Forcing of Atlantic Equatorial and Subpolar millennial cycles by precession, *Science, 274*, 1867–1870, 1996.

Mikolajewicz, U., A meltwater induced collapse of the 'conveyor belt' - Thermohaline circulation and its influence on the distribution of $\Delta^{14}C$ and $\delta^{18}O$, *Tech. Rep. 189*, 25 pp., Max-Planck-Inst. für Meteorol., Hamburg, Germany, 1996.

Mikolajewicz, U., T. J. Crowley, A. Schiller, and R. Voss, Modelling teleconnections between the North Atlantic and North Pacific during the Younger Dryas, *Nature, 387*, 384–387, 1997.

Mook, W. G., ^{13}C in atmospheric CO_2, *Netherlands J. Sea. Res., 20*, 211–223, 1986.

Najjar, R. G., J. L. Sarmiento, and J. R. Toggweiler, Downward transport and fate of organic matter in the ocean: Simulations with a general circulation model, *Global. Biogeochem. Cycles, 6*, 45–76, 1992.

Oeschger, H., J. Beer, U. Siegenthaler, B. Stauffer, W. Dansgaard, and C. C. Langway, Late glacial climate history from ice cores, in *Climate Processes and Climate Sensitivity, Geophys. Monogr. Ser., vol. 29*, edited by J. E. Hansen and T. Takahashi, pp. 299–306, AGU, Washington, D. C., 1984.

Peteet, D., Global Younger Dryas?, *Quat. Int., 28*, 93–104, 1995.

Rau, G. H., T. Takahashi, and D. J. D. Marais, Latitudinal variations in plankton $\delta^{13}C$: Implications for CO_2 and productivity in past oceans, *Nature, 341*, 516–518, 1989.

Schiller, A., U. Mikolajewicz, and R. Voss, The stability of the North Atlantic thermohaline circulation in a coupled ocean-atmosphere general circulation model, *Clim. Dyn., 13*, 325–347, 1997.

Severinghaus, J. P., T. Sowers, E. J. Brook, R. B. Alley, and M. L. Bender, Timing of abrupt climate change at the end of the Younger Dryas interval from thermally fractionated gases in polar ice, *Nature, 391*, 141–146, 1998.

Siegenthaler, U., and H. Oeschger, Biospheric CO_2 emissions during the past 200 years reconstructed by convolution of ice core data, *Tellus, Ser. B, 39*, 140–154, 1987.

Singer, C., J. Shulmeister, and B. McLea, Evidence against a significant Younger Dryas cooling event in New Zealand, *Science, 281*, 812–814, 1998.

Sowers, T., and M. Bender, Climate records covering the last deglaciation, *Science, 269*, 210–213, 1995.

Steig, E. J., E. J. Brook, J. W. C. White, C. M. Sucher, M. L. Bender, S. J. Lehman, D. L. Morse, E. D. Waddington, and G. D. Clow, Synchronous climate changes in Antarctica and the North Atlantic, *Science, 282*, 92–95, 1998.

Stocker, T. F., The seesaw effect, *Science, 282*, 61–62, 1998.

Stocker, T. F., Past and future reorganisations in the climate system, *Quat. Sci. Rev.*, 1999 (in press).

Stocker, T. F., and D. G. Wright, Rapid changes in ocean circulation and atmospheric radiocarbon, *Paleoceanography, 11*, 773–796, 1996.

Stocker, T. F., and D. G. Wright, The effect of a succession of ocean ventilation changes on radiocarbon, *Radiocarbon, 40*, 359–366, 1998.

Stocker, T. F., D. G. Wright, and L. A. Mysak, A zonally averaged, coupled ocean-atmosphere model for paleoclimate studies, *J. Clim., 5*, 773–797, 1992a.

Stocker, T. F., D. G. Wright, and W. S. Broecker, The influence of high-latitude surface forcing on the global thermohaline circulation, *Paleoceanography, 7*, 529–541, 1992b.

Thompson, L. G., T. Yao, M. E. Davis, K. A. Henderson, E. Mosley-Thompson, P.-N. Lin, J. Beer, H.-A. Synal, J. Cole-Dai, and J. F. Bolzan, Tropical climate instability: The last glacial cycle from a Qinghai-Tibetan ice core, *Science, 276*, 1821–1825, 1997.

Toggweiler, J., and B. Samuels, Is the magnitude of the deep outflow from the Atlantic Ocean actually governed by southern hemisphere winds ?, in *The Global Carbon Cycle*, edited by M. Heimann, pp. 303–331, NATO ASI Ser., Ser. I, 15, Springer Verlag, 1993.

Veum, T., E. Jansen, M. Arnold, I. Beyer, and J.-C. Duplessy, Water mass exchange between the North Atlantic and the Norwegian Sea during the past 28,000 years, *Nature, 356*, 783–785, 1992.

Weyl, P., The role of the ocean in climatic change: a Theory of the ice ages, *Meteorol. Monogr. 8*, 37–62, 1968.

Wright, D. G., and T. F. Stocker, Sensitivities of a zonally averaged global ocean circulation model, *J. Geophys. Res., 97*, 12,707–12,730, 1992.

Wright, D. G., and T. F. Stocker, Younger Dryas experiments, in *Ice in the Climate System*, edited by W. R. Peltier, pp. 395–416, NATO ASI Ser., Ser. I, 12, Springer Verlag, 1993.

Wright, D. G., T. F. Stocker, and D. Mercer, Closures used in zonally averaged ocean models, *J. Phys. Oceanogr., 28*, 791–804, 1998.

O. Marchal, T. F. Stocker, and F. Joos, Climate and Environmental Physics, Physics Institute, University of Bern, 5 Sidlerstraße, CH-3012 Bern, Switzerland. (e-mail: marchal@climate.unibe.ch; stocker@climate.unibe.ch; joos@climate.unibe.ch)